Doppler Aliasing Reduction In Wide-Angle Synthetic Aperture Radar Using A Linear Frequency Modulated Random Stepped-Frequency Waveform

THESIS

Jason McMahon, Captain, USAF

AFIT/GE/ENG/05-11

DEPARTMENT OF THE AIR FORCE
AIR UNIVERSITY

AIR FORCE INSTITUTE OF TECHNOLOGY

Wright-Patterson Air Force Base, Ohio

The views expressed in this thesis are those of the author and do not reflect the official policy or position of the United States Air Force, Department of Defense, or the United States Government.

AFIT/GE/ENG/05-11

Doppler Aliasing Reduction In Wide-Angle Synthetic Aperture Radar Using A Linear Frequency Modulated Random Stepped-Frequency Waveform

THESIS

Presented to the Faculty

Department of Electrical and Computer Engineering

Graduate School of Engineering and Management

Air Force Institute of Technology

Air University

Air Education and Training Command

In Partial Fulfillment of the Requirements for the

Degree of Master of Science in Electrical Engineering

Jason McMahon, B.S.E.E.

Captain, USAF

March 2005

AFIT/GE/ENG/05-11

Doppler Aliasing Reduction In Wide-Angle Synthetic Aperture Radar Using A Linear Frequency Modulated Random Stepped-Frequency Waveform

Jason McMahon, B.S.E.E.

Captain, USAF

Approved:

/signed/	9 Mar 2005
Maj Todd B. Hale, PhD (Chairman)	date
/signed/	9 Mar 2005
Dr. Michael A. Temple (Member)	date
/signed/	9 Mar 2005
Dr. Stephen C. Cain (Member)	date

AFIT/GE/ENG/05-11

Abstract

This research examines the theory, application, and results of using Random Stepped-Frequency (RSF) waveforms to mitigate Doppler aliasing in a *wide-angle* Synthetic Aperture Radar (SAR) imaging scenario. Severe Doppler aliasing typically occurs in this scenario since range extent requirements force the pulse repetition frequency to a value violating the lower bound for Doppler aliasing. Building on previous research, this work expands upon RSF waveform analysis using a Linear Frequency Modulated RSF (LFM-RSF) waveform. The RSF waveform suppresses Doppler aliasing by positioning nulls at the aliased scatterer location. Applying LFM with RSF processing theoretically provides greater frequency coverage and aliased scatterer cancellation improvement when compared to fixed frequency values. Results using the LFM-RSF waveform show images with alias mitigation performance consistent with previous non-LFM RSF results. Given a 45 dB image dynamic range and satisfying a time-bandwidth product criterion, the LFM-RSF waveform produces an image with aliased energy reduced by 99.6%. Slightly more energy reduction is possible by violating the time-bandwidth product criterion with an associated frequency overlap between subpulses. This violation leads to additional frequency coverage which enhances aliased energy reduction to 99.9%.

Acknowledgements

I would like to thank all who supported me in my thesis undertaking and in my entire AFIT experience. My thesis advisor, Maj Todd Hale, was instrumental in guiding me through the rough waters of AFIT from start to finish. His dedication to excellence contributed to my success. He filled in the gaps technically and practically. I would also like to thank Capt Jon Luminati for his time in helping me understand my thesis topic. In addition, Mr. Ed Zelnio (AFRL/SNA) deserves acknowledgements for originating the idea for my research (Wide-Angle Synthetic Aperture Radar).

On a personal note, my friends at AFIT were crucial to my survival. They kept moods light when school was intense. Most of all, I would like to express sincere gratitude and heartfelt affection for my wife. She will be happy to have me back in reality.

Jason McMahon

Table of Contents

Page

List of Figures

List of Tables

List of Symbols

Symbol		Page
f_d	Doppler frequency shift	7
v_r	Relative velocity	7
λ	Carrier signal wavelength	7
v_a	Instantaneous velocity	7
θ	Angle between platform and scatterer	7
δ_x	Range resolution	9
c	Speed of light	9
T	Pulse width	9
B	System bandwidth	9
τ	Compressed pulse width	9
B_c	Bandwidth of compressed pulse width	9
δ_y	Cross-Range (azimuth) resolution	11
D	Horizontal diameter of platform antenna	11
R	Range to target	11
$\Delta\theta$	Total viewing angle between platform and scatterer	12
$\Delta\phi$	Angular antenna beamwidth	13
L	Synthetic aperture length	14
$p(x, y)$	Scatterer locations	15
$\delta(x, y)$	Delta function	15
x_i	Scatterer location on x-axis	15
y_i	Scatterer location on y-axis	15
$\overline{\omega}$	Normalized Doppler frequency shift	17
$t_{\min}$	Minimum time delay	20
$t_{\max}$	Maximum time delay	20
$r(t)$	Received signal	21

Symbol		Page
$h(t)$	Matched filter impulse response	21
$y(t)$	Range profile	21
$s(t)$	Transmitted signal	22
f_c	Carrier signal frequency	22
T_r	Scatterer time delay	22
t_m	Matched filter time delay	23
T_{rs}	Reference scatterer time delay	23
f_{rs}	Reference scatterer Doppler frequency shift	23
k_r	Wavenumber of bandpass signal	26
θ	Viewing angle between platform and reference scatterer	26
$D(X, Y)$	Scene frequency data	26
$p_\theta(u)$	1-D Projection function	26
$h(\rho)$	Filtering kernel	27
$d(x, y)$	Terrain patch image	27
P_θ	Fourier transform of 1-D projection function p_θ	29
Q	Fourier Transform of the filtered projection function $q(u)$	29
u	Range transformation equation	30
$\hat{d}(x, y)$	Terrain patch image estimate	30
N	Number of subpulses in an RSF Waveform	42
$\lvert\chi(T_r, f_d)\rvert^2$	Ambiguity Function	42

List of Abbreviations

Abbreviation		Page
SAR	Synthetic Aperture Radar	1
WA-SAR	Wide Angle SAR	1
CW	Continuous Wave	1
LFM-RSF	Linear Frequency Modulated Random Stepped-Frequency	1
PRF	Pulse Repetition Frequency	1
CPI	Coherent Processing Interval	3
ISAR	Inverse SAR	6
SNR	Signal-to-Noise Ratio	21
FFT	Fast Fourier Transform	30
PRI	Pulse Repetition Interval	32
AF	Ambiguity Function	33
RSF	Random Stepped-Frequency	40

Doppler Aliasing Reduction In Wide-Angle Synthetic Aperture Radar Using A Linear Frequency Modulated Random Stepped-Frequency Waveform

I. Introduction

Historically, due to technology limitations, Synthetic Aperture Radar (SAR) designers chose between coverage area and resolution. Imaging a large coverage area meant a reduction in resolution. Conversely, imaging at high resolution meant focusing on one particular patch of terrain. These situations describe the two primary SAR operational modes: stripmap and spotlight modes (more detail on these modes in the next chapter). Considering advances in technology, it is appropriate to attempt utilizing the benefits of both modes by employing Wide-Angle SAR (WA-SAR). WA-SAR platforms theoretically obtain a high resolution image spanning a considerable coverage area while in stripmap mode. Attaining this image gives rise to new problem areas not present if either mode was used independently.

1.1 Problem Statement

This research investigates the benefits of implementing a Continuous Wave (CW) Linear Frequency Modulated Random Stepped-Frequency (LFM-RSF) waveform in a WA-SAR system. This waveform's purpose is to more effectively suppress Doppler aliasing from the scene image. WA-SAR produces high resolution images while covering a large ground area. Doppler aliasing occurs in WA-SAR by not increasing the Pulse Repetition Frequency (PRF) to a value appropriate for a larger Doppler bandwidth. WA-SAR requires an increase in the antenna beamwidth, leading to an increase in Doppler bandwidth. The PRF has a lower bound proportional to the Doppler bandwidth to avoid Doppler aliasing. However, the required PRF to meet the lower bound in WA-SAR becomes unviable in practical SAR operational systems.

The research approach violates the PRF lower bound and mitigates the resulting Doppler aliasing through waveform design.

The process of validating WA-SAR theory begins with defining the SAR imaging scenario geometry. The SAR platform operates in stripmap mode with broadside collection only and a wide-angle radar beam. The platform moves through one synthetic aperture length to acquire the scene image. In the scene, there are numerous point scatterers placed at different ranges and Doppler shifts. For simulation purposes, there is one reference scatterer located at zero range and zero Doppler shift. The rest of the scene consists of point scatterers at different ranges and Doppler shifts in relation to this reference scatterer. From this scenario, the research experiments with different waveforms to examine how they affect the range profiles and scene images. The waveforms utilized in this research are LFM, RSF, LFM-RSF adhering to a time-bandwidth product, and LFM-RSF violating the time-bandwidth product.

1.2 Scope and Assumptions

The research focuses on the task of validating the proposed theory and designs the imaging scenario to accomplish this task rather than faithfully represent real-world situations. Such real-world situations unnecessarily complicating the imaging scenario include three-dimensional imaging, platform velocity changes, non-stationary scatterers, electromagnetic signal effects, and scene diversity between pulses. This section describes general assumptions while other chapters cover more specific additional assumptions (i.e., mathematical, etc.). Such specific assumptions are more appropriate in sections fully describing the topic.

As discussed previously, the SAR platform operates in stripmap mode and emits a broadside beam (no squint). Broadside refers to the situation where the SAR platform emits a radar beam in a direction orthogonal to its motion. Squint refers to the radar beam being transmitted in a direction other than orthogonal to platform motion [2]. Chapter 2 discusses stripmap mode in detail.

The research also considers only a two-dimensional imaging scenario. Although real operational systems must handle a three-dimensional imaging situation, two-dimensional results are sufficient to validate the theory.

The first assumption is constant SAR platform velocity. In operational SAR systems, inertial navigation units can accurately measure platform speed. Processing methods then account for the changes in velocity.

Another assumption is stationary scatterers (scatterer velocity is zero). For the purposes of this research, a motionless target is sufficient to exhibit selected waveform effects and Doppler aliasing. Furthermore, the research only considers point scatterers. The drawback of using point scatterers is they do not represent real world complex scatterers such as tanks, aircraft, and artillery. Qualitatively, a point scatterer can be viewed as a target that exists at only one particular spot in the radar beam with unit height. Point scatterers also exhibit known effects when imaged by a SAR system.

Several assumptions are also made concerning electromagnetic radiation emitted by the antenna located on the WA-SAR platform. These assumptions dictate that there are no atmospheric effects on the radar beam (a lossless situation), planar far-field wavefronts, and perfect reflection. No atmospheric effects on the radar beam means the energy the antenna transmits stays constant throughout transmission and reflection. Planar wavefronts require assuming the target range is at a sufficient distance so that the spherical waves can be assumed planar [1]. Perfect reflection means the amount of energy incident to a scatterer is exactly the amount of energy reflected by the scatterer.

The final assumption concerns the synthetic array length, Coherent Processing Interval (CPI), and the distance between the SAR platform to the scatterers [8]. For range profiles to be coherently combined, the distance the SAR platform travels between pulses must be small when compared with the distance to the scatterers's location. This requirement assures the scene does not change significantly between

pulses, allowing the range profiles to be coherently combined. The WA-SAR scenario description in Chapter 2 justifies this assumption.

1.3 Thesis Organization

The thesis organizes each chapter using a building block approach. Each chapter's primary purpose is developing rational arguments towards investigating the proposed theory. The second chapter discusses fundamental WA-SAR concepts necessary to build a foundation for the research in this thesis. The third chapter reproduces results from [8] and validates the methodology and theory of RSF waveforms when applied to the SAR scenario. As an extension of the previous work, the fourth chapter examines the LFM-RSF waveform when applied to the same SAR scenario. The fifth chapter continues with the same waveform as in Chapter 4 with the exception of some modifications and presents its effects on the SAR imaging scenario. The modifications violate a time-bandwidth product improving frequency coverage and enhancing alias removal. Finally, the sixth chapter draws conclusions from the simulation results and offers recommendations for future research.

II. Literature Review/Background

Synthetic Aperture Radar (SAR) systems provide an all-weather, day or night imaging capability that is useful to a wide variety of organizations, including the military and intelligence community. In general terms, SAR systems use a moving platform to synthesize a large antenna array, increasing azimuth resolution to a point where image formation is possible. This moving platform periodically emits signals during a predetermined path length where the returned signals are coherently processed to produce an image. SAR enhances only the azimuth, or cross-range, resolution with no improvement in down-range resolution [2]. As in conventional radar, improvement in down-range resolution occurs via pulse compression. SAR systems typically generate a 2-D illuminated mapping of scatterers from returned signals.

This chapter contains descriptions of essential SAR topics that establish a foundation for the research described in this thesis. Included are descriptions of the SAR concept, pulse compression, Wide-Angle SAR (WA-SAR) imaging, WA-SAR research scenario, imaging technique theory and implementation, and results from the baseline Linear Frequency Modulated (LFM) SAR image. The last section in this chapter includes a preview of the remaining thesis document. Once this chapter establishes a foundation of SAR knowledge, Chapters 3, 4, and 5 expand on waveform concepts to accomplish effective Doppler aliasing reduction.

The topics in this chapter are essential to fully understand the applied methods and validate the proposed WA-SAR theory. The synthetic aperture concept is the elementary principle in SAR. Descriptions of SAR operational modes, Doppler effect, range ambiguities, range resolution, and cross range resolution assist in understanding SAR system concerns and how SAR forms images. WA-SAR description and limitations establish the primary issue with WA-SAR and the method to manage the limitation. Next, a scenario description illustrates the scene containing the terrain patch the WA-SAR system is trying to image. Understanding the geometry and Doppler characteristics of the scatterers in the scene aids in comprehending Doppler aliasing and why this aliasing occurs. In addition, the imaging algorithm reduces

computational loads permitting an efficient WA-SAR imaging scenario simulation. Finally, the LFM imaging case exhibits the Doppler aliasing in its images. These images show the effects of aliasing and serves as a comparison for cases with alias mitigation.

2.1 Synthetic Aperture Radar (SAR) Concept

The synthetic aperture concept is the basis for SAR operation. Without a synthetic aperture, the desired cross-range resolution for imaging would not be attainable in a physically realizable system. Assuming a single radiating element on a moving platform, the antenna transmits a signal at specific positions in time towards the terrain of interest. The antenna usually transmits a radar beam perpendicular to the flight path. However, it can also transmit radar beams at other angles and even focus on a particular terrain patch. After the signal reflects off scatterers, the antenna receives the returned signal. Typically, SAR processing digitally stores the returned signals' amplitude and phase for later computation. Conversely, a SAR imaging algorithm called Back-Projection processes radar returns serially. Shown later in this chapter, such serial processing results in substantial memory reduction. After the SAR platform has covered the length of the synthetic aperture, the stored radar return signals are similar to the radar return signals from an equivalent length real, physical antenna. The equivalent physical antenna size equals the synthetic aperture length [2]. This similarity allows synthesizing a long antenna array aperture from a short physical antenna. Individual pulses in the synthetic array act as distinct elements in a real, physical antenna array.

2.1.1 SAR Operational Modes. Describing SAR operational modes enlighten the motivations for attempting WA-SAR. WA-SAR utilizes the benefits of two popular SAR modes. SAR usually operates in four modes including stripmap, spotlight, scan, and Inverse SAR (ISAR) [13]. In stripmap mode, the antenna emits a beam along a strip of terrain parallel to the path of motion. In spotlight mode, the sensor steers

its antenna beam to continuously illuminate a specific terrain patch. Scan mode occurs when the sensor steers the antenna beam to illuminate a strip of terrain at any angle to the path of motion. The fourth mode is ISAR [11]. In ISAR, the radar is stationary with the scatterer moving around the radar. Laboratory experiments and naval applications commonly use ISAR.

For WA-SAR, stripmap and spotlight are the modes of interest. The advantage of stripmap mode is a wide coverage area. The major advantage of spotlight mode is resolution. In spotlight mode, the scatterer remains in the radar beam for a longer period of time than stripmap, allowing a longer synthetic array. Therefore, it yields a resolution increase. The disadvantage of spotlight mode is limited coverage area. WA-SAR attempts to adaptively focus on scatterers within the radar beam to achieve spotlight mode quality images while operating in stripmap mode; gaining the advantages of both modes.

2.1.2 Doppler Effect. The Doppler frequency shift is a major factor in SAR processing. Platform motion causes a change in antenna position and induces Doppler frequency shifts in the echo signals. Referring to [11], Doppler frequency shift f_d is given by

$$f_d = \frac{2v_r}{\lambda} \tag{2.1}$$

$$= \frac{2v_a \cos\theta}{\lambda}, \tag{2.2}$$

where v_r is the relative velocity, λ is the wavelength of the transmitted signal, v_a is the instantaneous SAR platform speed, and θ is the angle between the platform's velocity vector and scatterer. The relative velocity changes as the angle changes between radar platform and scatterer. Doppler frequency shift is the amount of frequency change in an echo signal when compared to the transmitted signal frequency.

Doppler frequency shift aids in correct focusing of scatterers in SAR images. Focusing of scatterers depends on phase information in the returned signal. Doppler

frequency shift causes a returned signal phase shift. This phase information determines image *cross-range* position for a scatterer. Assuming a stationary scatterer, if correctly acquired and processed, the returned signal's phase dictates the scatterer's true cross-range location in the SAR image. SAR imaging algorithms only map motionless scatterers to their true positions [2]. If the scatterers are moving during the Coherent Processing Interval (CPI), the movement induces errors in SAR image scatterer location.

2.1.3 Range Ambiguities. Range ambiguities are usually a concern for conventional radar, but are not a consideration in this WA-SAR scenario. SAR inherently shields itself against range ambiguities by concentrating on specific terrain patches in the scene and compensating for the ambiguous return's azimuth history. These reasons illustrate an important difference between SAR and conventional radar.

Since the SAR platform is either airborne or spaceborne, it illuminates only the unambiguous range interval with its radar beam [4]. This choice of imaging terrain patch illustrates a fundamental difference in the purpose for SAR versus conventional radar. In conventional radar, the radar's primary purpose is *detection* of scatterers while in SAR the primary purpose is to *image* a terrain patch. This research utilizes a Continuous Wave (CW) signal which results in all ranges being ambiguous. The range becomes unambiguous through LFM. Also, there is a distinct difference between azimuth (phase) histories of an ambiguous range scatterer when compared to an unambiguous range scatterer [4]. Signal processing techniques can then take advantage of this difference and remove the ambiguous scatterers.

2.1.4 Range Resolution. Another significant issue with SAR is range resolution. Range resolution improvements in both SAR and conventional radar result from employing pulse compression techniques. The synthetic aperture concept only improves cross-range (azimuth) resolution. SAR does *nothing* to improve range resolution. The following discussion justifies the implementation of pulse compression techniques in the WA-SAR scenario.

The definition for resolution is the smallest amount of relative distance required between neighboring scatterers to consider the scatterers distinct [2]. Assuming no pulse compression, radar improves range resolution by emitting a shorter pulse [11]. Again, assuming no pulse compression, the equation for radar range resolution δ_x is [11]

$$\delta_x = \frac{cT}{2}, \tag{2.3}$$

where c is the speed of light (300,000 km/s) and T is the pulse width. This equation highlights that a shorter pulse improves range resolution. Improvement in range resolution signifies a smaller value resulting from (2.3). Pulse width T is inversely proportional to system bandwidth B [11]. Therefore, a shorter pulse width results in a larger bandwidth and vice versa. From (2.3), range resolution without pulse compression improves by shortening the pulse width which leads to increasing system bandwidth. A shorter pulse also brings about power considerations by requiring undesirable higher peak power during transmission [11]. Increasing bandwidth requirements is also undesirable because of bandwidth limitations and an increase in receiver noise [11]. Adding more receiver noise results in an unwanted decrease in overall radar performance. Pulse compression is a method to improve range resolution maintaining acceptable peak power and bandwidth.

Pulse compression allows for a relatively long pulse width with a corresponding improvement in range resolution compared to range resolution of the same pulse without pulse compression. Pulse compression allows both sufficient power-on-target via a long pulse and adequate range resolution by increasing the spectral frequency band of the long pulse to match a shorter pulse's range resolution [11]. Pulse compression modifies the expression for range resolution in (2.3) to become

$$\delta_x = \frac{c\tau}{2} \tag{2.4}$$

$$= \frac{c}{2B_c}, \tag{2.5}$$

where τ is the compressed pulse duration and B_c is the compressed pulse bandwidth.

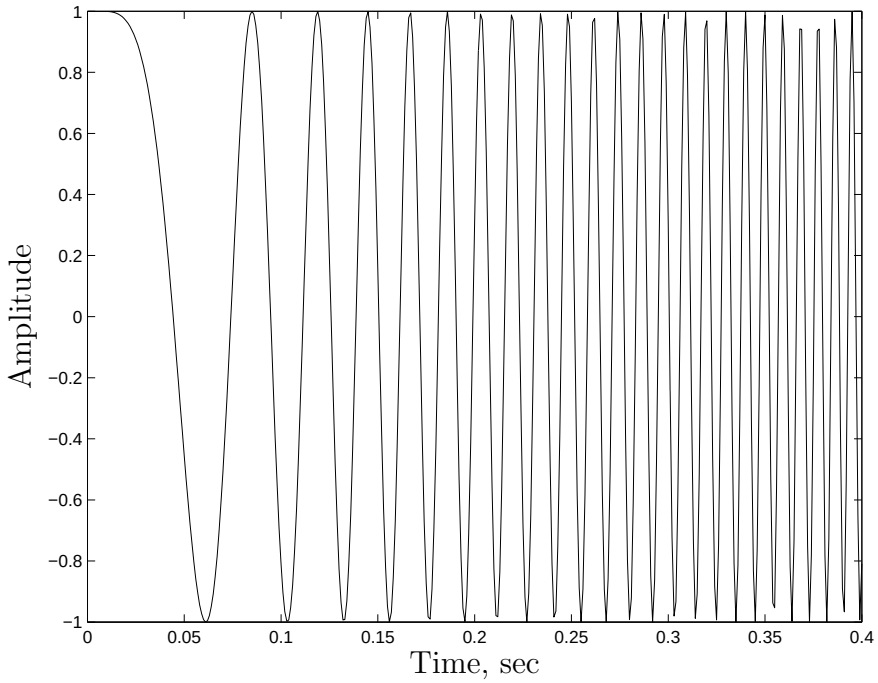

Figure 2.1: LFM Up-chirp signal. In an LFM Up-chirp, the frequency linearly increases as time increases.

A commonly used pulse compression technique is an LFM waveform [2]. LFM compresses the pulse through linearly increasing (up-chirp) or decreasing (down-chirp) frequency over the duration of the pulse width [5]. Examples of up-chirp and down-chirp signals can be seen in Figs. 2.1 and 2.2, respectively. Upon receiving the echo signal, the receiver passes the frequency-modulated signal through a pulse-compression filter that compresses the frequency modulated return signal [11].

This research uses LFM waveforms in WA-SAR to obtain a baseline image through summation of processed range profiles. LFM waveforms do allow Doppler aliasing in WA-SAR because they do not contain the characteristics of random stepped-frequency waveforms that mitigate Doppler aliasing. All other waveforms in this thesis document compare against this baseline image to see how effective these other waveforms are in suppressing Doppler aliasing. Considering the popularity of LFM in SAR, establishing LFM as the baseline case is appropriate. Comparisons in future chapters between this baseline case and other waveforms are necessary to establish efficacy of the other waveforms at reducing Doppler aliasing.

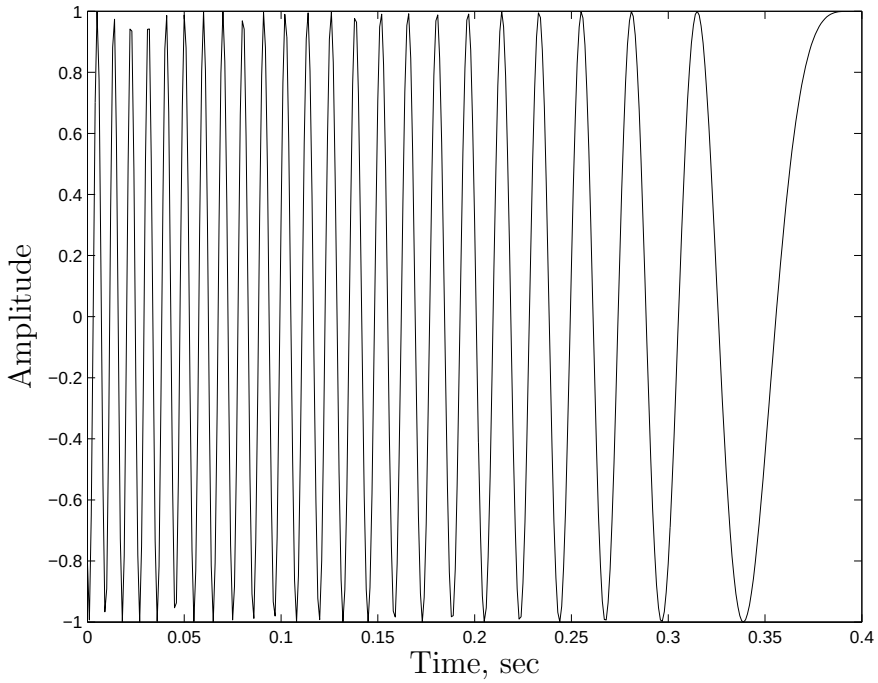

Figure 2.2: LFM Down-chirp signal. In an LFM Down-chirp, the frequency linearly decreases as time increases.

2.1.5 Cross-Range Resolution. SAR systems produce images and must incorporate methods to improve both range and cross-range resolution. Finer resolutions in SAR produce better images. As stated in the previous section, SAR improves *range* resolution by pulse compression. This section discusses improvement in *cross-range* resolution resulting from the synthetic aperture concept.

The benefit of SAR is significant cross-range resolution improvement. Conventional radar improves cross-range resolution via emitting a narrower beam [11]. Cross-range resolution improves as cross-range antenna beamwidth decreases. The cross-range resolution δ_y achievable by a conventional radar is [12]

$$\delta_y = \frac{R\lambda}{D}, \tag{2.6}$$

where D is the horizontal diameter of the antenna, R is the range to target, and λ is the carrier wavelength. Narrowing the beam (enlarging the antenna diameter) results in finer cross-range resolution. However, the requirement for cross-range resolutions

make using conventional radar impractical for imaging purposes. Consider a 3 m cross-range resolution in a conventional X-Band (10 GHz) imaging radar at a range of 10 kilometers. This situation requires an antenna diameter of 100 meters! Given that SAR platforms are typically satellites or airplanes, an antenna diameter of 100 meters is not physically realizable.

In SAR, the synthetic aperture allows the moving radar platform to achieve finer cross-range resolution than its real antenna beamwidth [2]. Using the small-angle approximation $\sin(\delta\theta) = \delta\theta$, the cross-range resolution achievable by a synthetic aperture is [5]

$$\delta_y = \frac{\lambda}{2\Delta\theta}, \tag{2.7}$$

where $\Delta\theta$ is the total viewing angle between the SAR platform and the scatterer as illustrated in Fig. 2.3. Equation (2.7) assumes spotlight mode operation. Although the platform is moving as though in stripmap mode, the SAR system in this research adaptively focuses on a single scatterer throughout the aperture length. This adaptive focusing specifies the spotlight mode definition for cross-range resolution. Also, although the viewing angle contains an implicit dependence on range, scatterers at different ranges only require an increase or decrease in viewing angle $\Delta\theta$ for equivalent resolution. Using the same scenario as described above, a SAR system requires a viewing angle $\Delta\theta$ of 0.286^o to achieve a 3 m cross-range resolution.

2.2 Wide-Angle SAR (WA-SAR) Description and Limitations

This section broadly describes WA-SAR and its limitations. Typically in stripmap mode, scatterers stay within the SAR antenna beam long enough to be resolved, but not long enough to obtain high resolution. SAR increases its cross-range resolution for a scatterer by increasing the time the scatterer is in the radar beam [2]. This cross-range resolution increase is due to more radar returns to synthesize into a longer synthetic array depicted by (2.7). Hence, if the angle of the transmitted radar beam

is increased as in WA-SAR, a given scatterer remains inside the beam longer and radar cross-range resolution improves.

Another benefit of WA-SAR imaging is the ability to choose which scatterer to focus on in the transmitted radar beam. Depending on scatterer choice and as long as the scatterer remains in the radar beam, SAR processing can choose to focus on the scatterer for the entire synthetic aperture length. This focusing leads to images of spotlight mode quality and processing of radar returns similar to spotlight mode processing.

However, there are several drawbacks to increasing the angular beamwidth of the transmitted signal. One drawback is the amount of data returned to the radar receiver is increased dramatically. This research uses an imaging algorithm that decreases the negative effect of this data increase. The research imaging algorithm, Back-Projection, processes SAR return signals serially which results in a dramatic decrease in memory requirements.

The other drawback leads to the motivation to investigate waveform performance in WA-SAR. From increasing the angular antenna beamwidth $\Delta\phi$, there is an associated increase in the Doppler bandwidth of the echo signals. This relationship originates from the following inequality between Pulse Repetition Frequency (PRF) and angular antenna beamwidth [2]

$$\text{PRF} \geqslant \frac{4v_a \sin(\Delta\phi/2)}{\lambda}, \tag{2.8}$$

where PRF is the inverse of the pulse width T. The expression on the right-hand side of (2.8) represents Doppler bandwidth. From this equation, Doppler bandwidth of the echo signals in SAR imaging provides the PRF lower bound. If the PRF cannot meet this lower bound, then Doppler aliasing results in the imaging process. WA-SAR, by definition, increases the angular antenna beamwidth $\Delta\phi$. Increasing beamwidth to satisfy WA-SAR requirements increases the Doppler bandwidth of the echo signals to a level that practical systems cannot employ radars at the PRF dictated by (2.8).

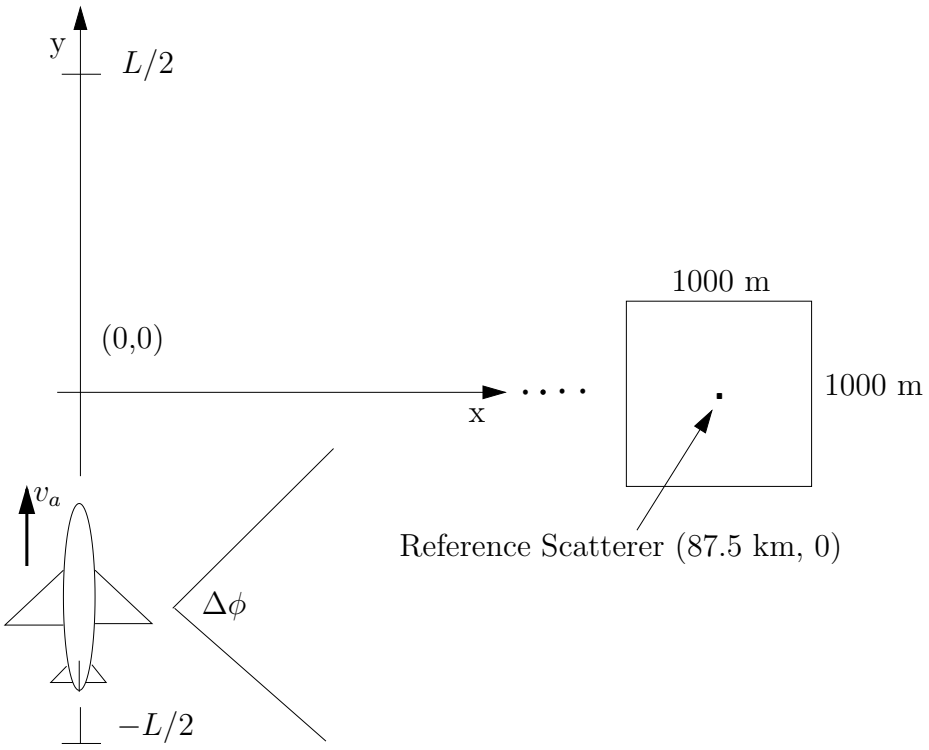

Figure 2.3: SAR Scenario Geometry. This figure shows the WA-SAR scenario. The scene center is at the center of the y, or cross-range, axis. L is the synthetic aperture length. $\Delta\phi$ is the angular beamwidth and v_a is the aircraft velocity.

An effective method to mitigate the issues of PRF and Doppler bandwidth in WA-SAR is to violate the lower bound given by (2.8) and select waveforms that are effective in suppressing the resulting Doppler aliasing. It turns out that Random Stepped-Frequency (RSF) waveforms exhibit qualities mitigating this aliasing. Chapters 3, 4, and 5 discuss alias reduction specifics.

2.3 Wide-Angle SAR Scenario Description

In this scenario, a WA-SAR platform flies a linear flight path along a synthetic aperture length of $L = 200$ meters. This platform's mission is to use WA-SAR to obtain a high resolution image of one point scatterer, reference scatterer, located in the scene. Figure 2.3 shows the platform orientation and the orthogonal movement relative to the terrain patch of interest. Table 2.1 presents the general simulation

Table 2.1: General Simulation Parameters

Parameter	Symbol	Value
Center Frequency	f_c	10 GHz
Pulse Repetition Frequency	PRF	2,000 Hz
Pulse Width	T	500 μsec
Bandwidth	B	20 MHz
Beamwidth	$\Delta\phi$	90^o
Minimum Range	$R_{\min}$	75,000 m
Maximum Range	$R_{\max}$	100,000 m
Range Swath	R_{sw}	25,000 m
Synthetic Aperture Length	L	200 m
Platform Velocity	v_a	100 or 200 m/s
2-D Scene Dimensions		1000 m $\times$ 1000 m
Scene Size		512 $\times$ 512 pixels

parameters. The SAR platform is flying as though it was in stripmap mode. However, the SAR processing only focuses on the reference scatterer. This focusing results in a spotlight mode quality image even though the platform is flying as though in stripmap mode. The WA-SAR benefits from advantages of both modes.

The scene consists of nine point scatterers with varying range from the platform. Refer to Fig. 2.4 and Table 2.2 for a Down-Range vs. Cross-Range graphical representation of the overall scene and the corresponding numerical locations, respectively. Figures 2.3 and 2.4 show the coordinate system used by the simulation to accurately locate the scatterers in the scene. The scatterers $p(x, y)$ are all unit magnitude at the following coordinate locations

$$p(x, y) = \sum_{i=1}^{9} \delta(x_i, y_i) \tag{2.9}$$

where $\delta(x, y)$ is a delta function and x_i and y_i are the coordinate locations for the nine scatterers corresponding to Table 2.2. The symbol $*$ denotes the reference scatterer in the table. A minor warning to the reader concerning notation. The delta function is $\delta(x_i, y_i)$ while δ_x and δ_y refer to range resolution. The coordinate system set-up allows the simulation to accurately calculate time delay and Doppler shift of individual

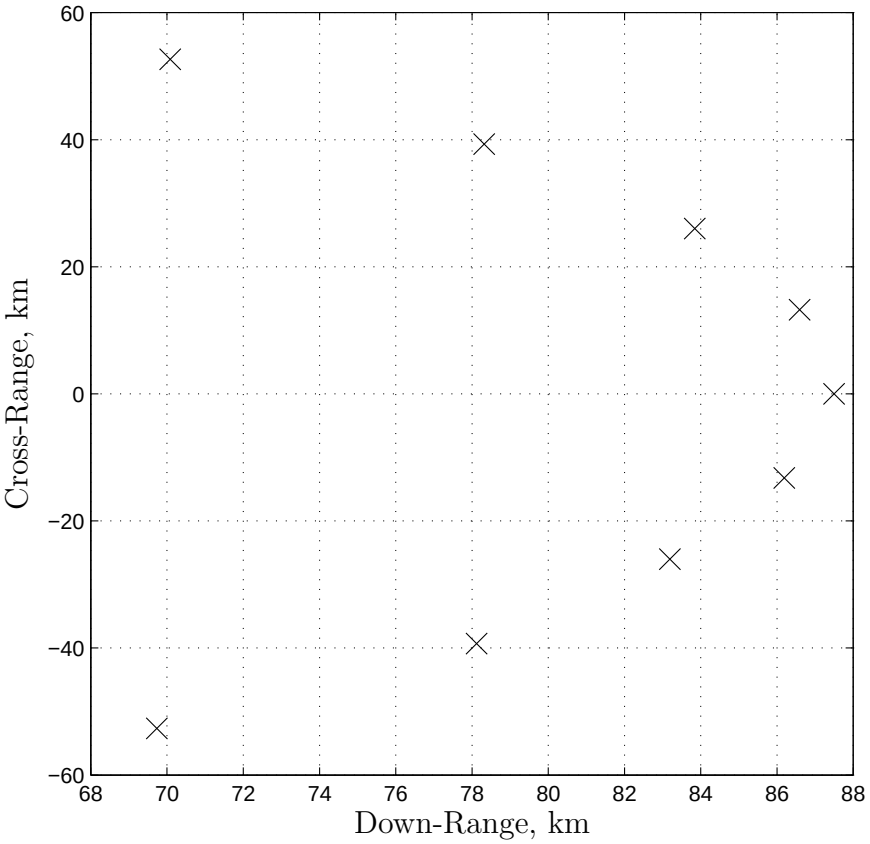

Figure 2.4: Scatterer Locations. The locations marked by an "x" are the scatterer locations with the reference scatterer at 87.5 km in Down-Range and 0 m in Cross-Range. Considering the synthetic aperture length $L = 200$ m, the angular antenna beamwidth $\Delta\phi = 90^o$, and the range to the scatterers, these scatterers are never outside of the radar beam during the entire synthetic aperture length.

Table 2.2: Scatterer Range Parameters

Scatterer	Down-Range (m)	Cross-Range (m)
1	70,081	52,659
2	78,320	39,315
3	83,842	26,020
4	86,593	13,235
5*	87,500	0
6	86,193	-13,235
7	83,192	-26,022
8	78,120	-39,315
9	69,731	-52,659

Table 2.3: Scatterer Normalized Doppler Parameters

	Normalized Doppler ($\overline{\omega}$) (Hz)	
Scatterer	100 m/s	200 m/s
1	2.00	4.00
2	1.50	2.99
3	0.99	1.98
4	0.50	1.00
5	0	0
6	-0.51	-1.01
7	-1.00	-1.99
8	-1.50	-3.00
9	-2.01	-4.02

scatterers as the platform flies along the synthetic aperture. The terrain patch of interest is 1000 meters by 1000 meters with the reference scatterer in the center of this patch at 87 km in down-range and 0 km in cross-range.

Assuming the moving platform is at the center of the coordinate system (refer to Fig. 2.3), Table 2.3 shows the resultant normalized Doppler frequency shift $\overline{\omega}$ of each scatterer with respect to the reference scatterer. The equation for $\overline{\omega}$ is

$$\overline{\omega} = \frac{f_d}{\text{PRF}}. \tag{2.10}$$

Data in Table 2.3 is crucial in explaining why Doppler aliasing occurs. Since Doppler aliasing occurs at integer multiples of the PRF [11], this table shows which individual scatterers, depending on platform velocity, alias into the image of the terrain patch. This aliasing shows up later in this chapter when looking at image formation.

An important parameter for an imaging system is resolution. Resolution requirements are reasonable since resolution improvement is not the goal of this research.

Equation (2.4) determines this SAR system's down-range resolution to be

$$\begin{aligned} \delta_x &= \frac{c}{2B} \\ &= \frac{300,000 \text{ km/s}}{2(20 \text{ MHz})} \\ &= 7.5 \text{ m}. \end{aligned} \tag{2.11}$$

Equation (2.7) establishes the SAR system's cross-range resolution as

$$\begin{aligned} \delta_y &= \frac{\lambda}{2\Delta\theta} \\ &= \frac{0.03 \text{ m}}{2(0.0023 \text{ rads})} \\ &= 6.56 \text{ m}. \end{aligned} \tag{2.12}$$

2.4 Imaging Technique - Back-Projection Algorithm

This section discusses the advantages of the simulation's imaging algorithm, Back-Projection, and the range profiles that generate the image, as well as the derivation and implementation of the algorithm. The simulation utilizes the Back-Projection algorithm to image the reference point scatterer. Other methods are available such as Polar Reformatting [5], but the advantages of using the Back-Projection algorithm are uniquely useful in this research. The simulation is purposefully set up to use these advantages to lighten the processing requirements.

2.4.1 Advantages. There are two primary advantages for using the Back-Projection algorithm. The first advantage is this algorithm processes radar signals in serial. In other words, for each synthetic aperture array location (i.e., each transmitted pulse), this algorithm processes the returned radar signal, or echo signal, from that specific synthetic aperture array location. Serial processing dictates processing of one synthetic aperture echo signal from one synthetic aperture location at a time. A tradeoff in performing serial processing is time duration. Since processing occurs on each echo signal, the simulation takes more time than if imaging the entire collection of

pulses at the same time. In this research, time duration is not a concern. The second advantage of this algorithm is the range extents of the image (portion of the scene being imaged) can be a subset of the entire range covered by the received signal. Specifying range extents further reduces the memory requirements. The previous section defines the image range extents, terrain patch of interest, as 1000 m by 1000 m. Considering the image range extents, the algorithm selects the corresponding time samples in the received signal to form the image. In radar, time delay translates to range using the relationship $R = ct/2$ [11]. Hence, not only does this algorithm process serially, but it also only needs a small portion of the entire received signal for image formation. The amount of data from a complete synthetic aperture length, $L = 200$, of a WA-SAR system is generally too large for most computers to effectively manipulate. The Back-Projection imaging algorithm reduces this data burden.

Investigating the size of the simulation's transmitted and received signals should clarify these advantages. The time samples of the transmitted and received signals are complex since they are defined by complex envelope notation. The reason to use complex envelope notation is because these signals are complex in real-world radar due to in-phase and quadrature channel processing [11]. Table 2.1 provides the parameter values for the SAR system. The sampling frequency for the transmitted and received signals satisfy Nyquist frequency sampling requirements by equalling twice the system bandwidth. With bandwidth at 20 MHz, the minimum Nyquist sampling frequency f_s equals 40 MHz. Sample time is then given by $t_s = 1/f_s$ which results in a sample time of 25 nsec. Considering a pulse width of $T = 500$ μsec, there are $20,000$ samples in each transmitted signal. At 16 bytes per complex sample in the simulation program, the transmitted signal at one synthetic aperture location requires 320 kilobytes. With 4000 synthetic aperture locations (assume aircraft velocity is 100 m/s), the memory requirements of the transmitted signal across the entire aperture is 1.28 Gigabytes. Clearly, there is a substantial size difference between one signal and the collection of signals from the synthetic aperture (320 kilobytes versus 1.28 Gigabytes).

For SAR purposes, the signal of interest for imaging is the received signal. A received signal is a modified version of the transmitted signal that bounces off a scatterer in the scene and returns to the radar. This signal is a time-delayed and frequency-shifted version of the transmitted signal. Time delay and frequency shift of a scatterer modifies the transmitted signal and defines the received signal for that scatterer. The range swath parameters determine the extent and size of the received signal which include the range swath at 25 km, the minimum range to the swath from the SAR platform $R_{\min}$ at 75 km, and maximum range extent of the swath from the SAR platform $R_{\max}$ at 100 km. From these parameters, a minimum and maximum time establishes the time extent of the received signal. The minimum time $t_{\min}$ is

$$t_{\min} = \frac{2R_{\min}}{c} \tag{2.13}$$

and maximum time $t_{\max}$ with T as the pulse width is

$$t_{\max} = \frac{2R_{\max}}{c} + T. \tag{2.14}$$

Using (2.13) and (2.14), the received signal time duration is 666.67 μsec which results in $26,666$ samples. Again, at 16 bytes per complex sample, a received signal from one synthetic aperture location requires 426.656 kilobytes. With 4000 synthetic aperture locations (assuming aircraft velocity is 100 m/s), the memory requirements of the received signal across the entire aperture is 1.71 Gigabytes. Processing one signal at a time, as in Back Projection, results in a 99.997% reduction in memory requirements.

Windowing the received signal further reduces memory requirements. However, the reduction due to windowing is marginal compared to the reduction due to serial processing. The $t_{\min}$ and $t_{\max}$ as defined by (2.13) and (2.14) define the received signal time extents. The associated minimum and maximum ranges covered by the received signal are $ct_{\min}/2 = 75$ km and $ct_{\max}/2 = 175$ km, respectively. Subtracting the maximum range from the minimum range gives the overall range covered by the received signal as 100 km. Referring to Table 2.1, the terrain patch covers 1000 m

in range and 1000 m in cross-range. This patch dictates that only 1000 m out of the 100 km require processing for imaging purposes. The entire received signal covers 100 km and consists of $26,666$ time samples. Range distance per sample is then 3.75 m/sample. Given this algorithm only requires 1000 m of time samples from each received signal, only 2,667 samples (42.67 kilobytes) are necessary for image formation.

The combination of serial processing and received signal windowing dramatically reduces memory requirements. The overall reduction memory is from 1.71 Gigabytes to 42.67 kilobytes: a 99.998% overall reduction in memory requirements.

2.4.2 Generating Range Profiles. A range profile in this research is the matched filter output from one synthetic aperture location. Each synthetic aperture location corresponds to one received signal. Each received signal contains a summation of the contributions from each individual scatterer. Individual scatterers generate their own received signal based on its time delay and Doppler frequency shift.

Matched filtering is appropriate given it achieves maximum Signal-to-Noise Ratio (SNR) [11]. Several assumptions allow the WA-SAR scenario to be considered a linear system with a known filter. A linear system contains an input $r(t)$, impulse response $h(t)$, and output $y(t)$. In this research, the composite received signal from each synthetic aperture location constitutes the input. The matched filter impulse response $h(t)$ is a flipped and conjugated version of the received signal for the reference scatter. The output of the system $y(t)$ is the range profile. Using the reference scatterer to define the matched filter specifies focusing on the reference scatterer by the WA-SAR system. If desired, SAR processing could choose another reference scatterer by using that scatterer's received signal to define the matched filter.

The SAR system focuses on this reference scatterer independent of platform physical location along the synthetic aperture. Even though the platform is flying as if in stripmap mode, it is this focusing on one motionless scatterer that enables spotlight mode quality resolution. Moreover, all mathematical development assumes

a spotlight mode situation. Additionally, Back-Projection is primarily a spotlight mode imaging algorithm.

Matched filtering requires several assumptions pertaining to the waveform and system. The primary assumptions are: known signal, additive white noise only, no distortion due to the environment in the received waveform relative to the transmitted waveform, optimization goal is maximum SNR, and system is linear, time-invariant, and stable [3]. The following mathematical expressions and associated discussion detail why these assumptions are important.

Assuming a complex envelope sinusoid, the following defines the transmitted signal $s(t)$ at unit amplitude as

$$s(t) = \begin{cases} e^{(j2\pi f_c t)} & 0 < t < T \\ 0 & \text{otherwise,} \end{cases} \tag{2.15}$$

where f_c is the carrier frequency. Equation (2.15) shows a typical complex envelope sinusoid notation. Regardless of chosen waveform, the following defines the received signal $r(t)$ from a specific scatterer having two way (platform to scatterer and back) time delay T_r and Doppler frequency shift f_d

$$r(t) = \begin{cases} s(t - T_r)e^{[j2\pi f_d(t-T_r)]} & T_r < t < T + T_r \\ 0 & \text{otherwise,} \end{cases} \tag{2.16}$$

where $T_r = R_s/c$ with R_s as the range to the specific scatterer. Time delay refers to the time it takes for the transmitted signal to propagate from the WA-SAR platform to a scatterer, reflect off of the scatterer (no distortion), and propagate back to the WA-SAR platform. Equation (2.1) defines the Doppler frequency shift f_d. Doppler frequency shift is the amount of the change in frequency the WA-SAR platform, given a synthetic aperture location, observes from a reflected signal off a scatterer.

Assuming the system is linear, time-invariant, and stable, there exists a filter $h(t)$ that produces maximum output SNR. Theoretically, assuming zero Doppler shift and a complex transmitted signal, the impulse response for this matched filter $h(t)$ is [11]

$$h(t) = \begin{cases} s^*(t_m - t) & t_m - T < t < t_m \\ 0 & \text{otherwise.} \end{cases} \tag{2.17}$$

where $*$ is the complex conjugate and t_m is the time required for causality. In other words, the matched filter impulse response is a flipped and shifted version of the transmitted waveform. Ideally, for conventional radar matched filtering, t_m is the pulse width. For this research, t_m is set as the time delay for the reference scatterer. Since there are range profiles generated for each synthetic aperture location, there exists a distinct $h(t)$ based on the time delay of the reference scatterer at each location. A Doppler frequency shift needs to be incorporated into the matched filter because the WA-SAR system is focusing on a scatterer having a nonzero Doppler shift throughout the aperture. The matched filter signal for this research is the flipped and conjugated version of the received signal for the reference scatterer. The reference scatterer time delay T_{rs} and Doppler shift f_{rs} define the research's matched filter as

$$h(t) = \begin{cases} \left[s(T_{rs} - t)e^{[j2\pi f_{rs}(T_{rs} - t)]}\right]^* & T_{rs} - T < t < T_{rs} \\ 0 & \text{otherwise.} \end{cases} \tag{2.18}$$

Since the system is linear, time-invariant, and stable, the output of the system is the convolution of the input $r(t)$ and the filter $h(t)$ [3]. The output of the system $y(t)$ is then

$$y(t) = r(t) \otimes h(t) \tag{2.19}$$

where $\otimes$ is the symbol for convolution. This range profile or matched filter output $y(t)$ is now ready for image formation processing by the imaging algorithm. A change

to the transmitted waveform also changes the received waveform and matched filter impulse response. However, the standard definitions from (2.16) and (2.18) remain constant. Different transmitted waveforms (i.e., LFM, stepped-frequency, etc.) behave similarly when applied to this system. Each waveform can define a received signal and a matched filter impulse response. Behavior of the linear system is waveform independent. This linear system model is applicable to every waveform in this research.

The final form of the matched filter output for the reference scatterer given by (2.18) is waveform independent. For example, assuming matched filtering on only this reference scatterer, the system consists of the matched filter impulse response $h(t) = r^*(T_r - t)$ and returned signal $r(t)$ with time delay T_r and Doppler shift f_d. Solving for the matched filter output gives

$$\begin{aligned} y(t) &= r(t) \otimes h(t) && (2.20) \\ &= s(t - T_r)e^{j2\pi f_d(t-T_r)} \otimes s^*(-t)e^{j2\pi f_d t} && (2.21) \\ &= \mathcal{F}^{-1}\left[\ \mathcal{F}[s(t - T_r)e^{j2\pi f_d(t-T_r)}]\mathcal{F}[s^*(-t)e^{j2\pi f_d t}\ \right], && (2.22) \end{aligned}$$

where Fourier Transform properties have been used. After performing the Fourier Transforms specified by the previous equation, the matched filter output magnitude becomes

$$|y(t)| = B\ \mathrm{sinc}[B(t - T_r)] \tag{2.23}$$

where B is the system bandwidth and $\mathrm{sinc}(x)$ is $\sin(\pi x)/\pi x$. The nulls of (2.23) occur at times equal to

$$t_{\text{nulls}} = \frac{n}{B} + T_r \tag{2.24}$$

where n equals nonzero integers (i.e., $\pm 1, \pm 2, \pm 3$, etc.). Converting the time of the first null to range using (2.24) and $R = ct/2$ results in a range resolution of 7.5 m. Equation (2.23) is valid for all scatterers when using the LFM waveform and for only the reference scatterer for the RSF waveforms. RSF waveforms attenuate scatterers

in the range profile based on $\text{sinc}(f_d T)$ [8]. Chapter 3 discusses this attenuation, or filtering, in more detail.

2.4.3 Derivation and Implementation. This part of Chapter 2 describes the derivation and implementation of the Back-Projection algorithm. The final product of this algorithm is an image that incorporates the echo signals from the entire synthetic aperture length. The final image is a summation of individual images from each synthetic aperture array location. Implementing this algorithm requires knowledge of basic radar fundamentals, matched filtering, sampling theory, Fourier Transforms, and interpolation techniques. Independent of waveform, this description explains how to derive the algorithm and then how to form images based on range profiles. A general description of the process is next in order to understand the complete picture before examining the details.

The process starts at the first location in the synthetic aperture array. The simulation produces a range profile at this location with the selected waveform and then performs image formation on this profile. The result of this first run is an image based on only one range profile. The simulation stores this first image for later summation with the image produced by the next synthetic aperture location. The simulation then steps to the second synthetic aperture location and generates a new image by performing the same image formation steps. Subsequently, summation occurs between the new image from the current range profile and the previous image from the first synthetic aperture location. The simulation then steps to the next synthetic aperture location, generates a new range profile, and forms a new image. Again, summation occurs between this individual image and the image resulting from summation between the previous two images. This process occurs for every synthetic aperture array location resulting in a final image that is the summation of all the individual images from the entire synthetic aperture array.

2.4.3.1 Derivation. This derivation follows the theory specified by [5]. The Back-Projection algorithm is a tomographic reconstruction method that today's

modern medical Computer Aided Tomography (CAT) scanners can implement to obtain medical images [5]. In SAR processing, image formation via Back-Projection is most common in spotlight mode SAR. The basis for the derivation of the Back-Projection algorithm is the projection slide theorem.

The beginning point of the derivation is the inverse Fourier Transform of the scene's frequency data $D(k_r \cos\theta, k_r \sin\theta)$ where k_r is the bandpass signal wavenumber and θ is the viewing angle between the platform and reference scatterer. In polar coordinates, the following equation expresses this inverse Fourier Transform [5]

$$d(\rho\cos\phi, \rho\sin\phi) = \frac{1}{4\pi^2}\int_{-\pi/2}^{\pi/2} d\theta \int_{-\infty}^{\infty} D(k_r\cos\theta, k_r\sin\theta)|k_r| e^{jk_r\rho\cos(\phi-\theta)} dk_r \quad (2.25)$$

where ρ and ϕ are polar coordinate variables for the cartesian coordinates x and y. The projection-slice theorem then modifies (2.25) into a practical expression for implementation. The projection-slice theorem permits the formation of the 2-D Fourier Transform $D(X, Y)$ of the reconstructed image from the 1-D Fourier transform of the projection function $p_\theta(u)$. The projection-slice theorem states that [5]

$$D(U\cos\theta, U\sin\theta) = P_\theta(U) \quad (2.26)$$

with

$$D(X, Y) = \int_{-\infty}^{\infty}\int_{-\infty}^{\infty} d(x, y) e^{[-j(xX+yY)]} dxdy \quad (2.27)$$

and

$$P_\theta(U) = \int_{-\infty}^{\infty} p_\theta(u) e^{(-juU)} du. \quad (2.28)$$

Equation (2.26) then becomes

$$D(k_r\cos\theta, k_r\sin\theta) = P_\theta(k_r) \quad (2.29)$$

in this derivation. Consequently, the projection-slice theorem substitutes (2.29) into (2.25) to result in

$$d(\rho\cos\phi, \rho\sin\phi) = \frac{1}{4\pi^2}\int_{-\pi/2}^{\pi/2} d\theta \int_{-\infty}^{\infty} P_\theta(k_r)|k_r| e^{[jk_r\rho\cos(\phi-\theta)]} dk_r \tag{2.30}$$

where $|k_r|$ requires an absolute value due to baseband signals. According to [10], convolution in the time domain is mathematically equivalent to multiplication in the Fourier domain. The integral on the righthand side of (2.30) is multiplication in the Fourier domain of $P_\theta(k_r)$ and $|k_r|$ where the Fourier relationships are $P_\theta(k_r) \leftrightarrow p_\theta(\rho)$ and $|k_r| \leftrightarrow h(\rho)$. Therefore, this integral is the convolution of a projection function $p_\theta(\rho)$ and a filtering kernel $h(\rho)$. Suppressing functional dependency, this Fourier Transform relationship is

$$P_\theta|k_r| \longleftrightarrow p_\theta \otimes h. \tag{2.31}$$

The convolution is a filter for the projection function p_θ. Setting $Q = P_\theta|k_r|$, the Fourier transform of Q is q equaling $p_\theta \otimes h$. The output of the convolution evaluated at $\rho\cos(\phi-\theta)$ results in

$$d(\rho\cos\phi, \rho\sin\phi) = \frac{1}{4\pi^2}\int_{-\pi/2}^{\pi/2} q(\rho\cos(\phi-\theta))d\theta. \tag{2.32}$$

Trigonometric identities transform the argument of q to

$$\rho\cos(\phi-\theta) = \rho\cos\theta\cos\phi + \rho\sin\theta\sin\phi = x\cos\theta + y\sin\theta. \tag{2.33}$$

Changing the argument of q to match (2.33) and substituting cartesian for polar coordinates in (2.32) with $x = \rho\cos\phi$ and $y = \rho\sin\phi$ results in

$$d(x, y) = \frac{1}{4\pi^2}\int_{-\pi/2}^{\pi/2} q(x\cos\theta + y\sin\theta)d\theta. \tag{2.34}$$

According to [5], the filtered projection function q defines the amplitude at each particular pixel location in $d(x, y)$. Figure 2.5 shows the patch of interest and projection

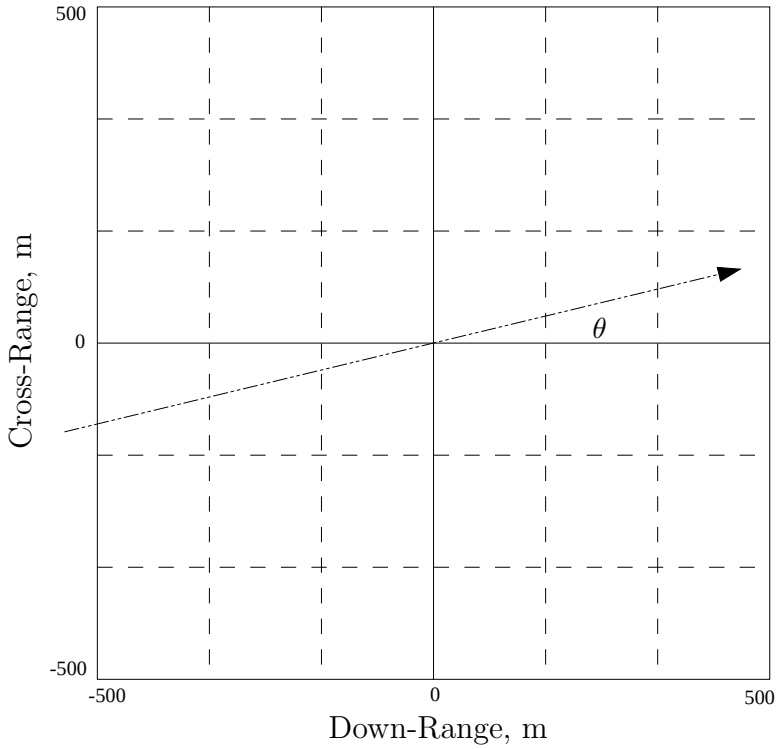

Figure 2.5: Terrain Patch of Interest. The Back-Projection algorithm uses the coordinate system of this figure to accurately place scatterers. As the platform propagates along the synthetic aperture, θ changes slightly as well. The SAR platform views the scatterer of interest for a total angular extent of 0.131^o.

function angle θ. Each of the pixel locations is the sum total of the amplitudes of the filtered projection function back-projected onto that pixel location. As outlined earlier in the chapter, it is this summation that allows for the drastic reduction in memory requirements. This reduction as well as ease of implementation make the Back-Projection algorithm an effective option for SAR imaging.

2.4.3.2 Implementation. Using the theory of Back-Projection, the simulation performs image formation on the raw range profile data from the WA-SAR scenario. This section describes the specific implementation steps to transform the raw data of the range profiles to the appropriate image of the terrain patch. This discussion is independent of waveform selection and scene scatterer locations.

Implementation begins with the following equation:

$$d(x,y) = \frac{1}{4\pi^2} \int_{-\pi/2}^{\pi/2} q(x\cos\theta + y\sin\theta)d\theta. \tag{2.35}$$

Derivation of the Back-Projection algorithm specifies the definition for q as

$$q = p_\theta \otimes h \tag{2.36}$$

or, equivalently,

$$q = \mathcal{F}^{-1}\left[P_\theta |k_r|\right], \tag{2.37}$$

where P_θ is the Fourier Transform of the range profile. For simulation purposes, the algorithm uses

$$\begin{aligned} q &= \mathcal{F}^{-1}\left[P_\theta |k_r|\right] && (2.38)\\ &= \mathcal{F}^{-1}\left[Q\right] && (2.39) \end{aligned}$$

to calculate the filtered projection function q. For each synthetic aperture location, P_θ is the Fourier Transform of the range profile. The variable $|k_r|$ is the wavenumber associated with the bandpass data from the bandwidth used by the WA-SAR platform: $f_c - B/2$ to $f_c + B/2$. The equation for wavenumber is $k_r = 4\pi/\lambda$. Sampling frequency determines the frequency increment in the bandwidth and, since frequency relates to wavelength by $\lambda = c/f$, each frequency increment then corresponds to a wavelength increment value. This array of wavelength values defines the vector k_r and, therefore, defines the filtered projection function

$$Q = P_\theta |k_r|. \tag{2.40}$$

At each synthetic aperture array location, the algorithm calculates Q via (2.40) and then performs an inverse Fourier Transform on Q to obtain the filtered projection function q. However, before this inverse Fourier Transform can occur, the Q func-

tion must be zero-padded at each synthetic aperture location. This zero-padding is necessary due to nonuniform spacing of the values in Q [9].

The filtered projection function q is a filtered version of the range profile p_θ. This function contains all the range and phase information of the scene at a particular θ angle. Figure 2.5 shows this θ azimuth angle in the geometry of the terrain patch. This angle changes as the WA-SAR platform travels along the synthetic aperture. At each synthetic aperture array location, there is a different θ value. The transformation equation u to go from a pixel value in the terrain patch to a range value in $q(u)$ is

$$u = x\cos\theta + y\sin\theta. \tag{2.41}$$

After transformation, a 1-D interpolation occurs on the filtered projection function $q(u)$ to obtain a new function at the range values specified by u. These range values back-project onto the estimated image $\hat{d}(x, y)$ at the same x and y values that define the transformation to calculate $q(u)$. In this research, the terrain patch forms a grid from -500 m to 500 m in both down-range (x values) and cross-range (y values). Formation of individual images take place by stepping through all possible combination of x and y locations in the grid and then identifying the appropriate magnitude from the q function.

Throughout implementation, the simulation utilizes a Fast Fourier Transform (FFT) routine that turns the original bandpass data ($f_c - B/2$ to $f_c + B/2$) into lowpass data [9]. For this reason, before summation can occur, the Fourier transform shifting property modifies the estimated image to make the low pass data into bandpass data once again.

At this point, the Back-Projection algorithm is complete. The individual scene is now ready for summation with other similarly processed scenes from other azimuth angles to contribute to total image formation.

2.5 Application of LFM Waveform

Using an LFM waveform under the scenario conditions listed in Tables 2.1 and 2.2, a WA-SAR platform transmits/receives radar signals and performs image formation on the received signals. LFM is the most common type of waveform utilized in SAR [5]. Additionally, several books, [2] and [13], utilize LFM in their basic SAR development. For these reasons, it is appropriate to begin this SAR research analysis with an LFM waveform.

Using an LFM waveform in this WA-SAR scenario causes several of the point scatterers to alias into the image when attempting to image only the reference scatterer. Geometrically, none of the other eight scatterers are *physically* located within the 1000 m by 1000 m box surrounding the reference scatterer. However, by choosing an LFM waveform, a few scatterers alias into the image because of their Doppler shift relative to the reference scatterer and PRF. Given that Doppler aliasing occurs at integer multiples of the PRF [11], Table 2.3 clarifies why scatterers appear in the image even though these same scatterers are not physically in the scene itself. In other words, those scatterers in Table 2.3 possessing integer values for $\overline{\omega}$, normalized Doppler frequency, alias into the SAR image.

Referring to Table 2.3, it is clear that scatterers 1, 3, 7, and 9 alias into the image at 100 m/s platform velocity. Similarly, for 200 m/s platform velocity, all scatterers alias into the image. Figures of the terrain patch support these statements later in the section.

2.5.1 Concept. The definition of the complex LFM transmitted signal is

$$s(t) = e^{\left\{j2\pi[(f_c - B/2)t + \alpha t^2]\right\}} \qquad 0 < t < T, \tag{2.42}$$

where f_c is the carrier frequency, B is the bandwidth, and α is the chirp rate. Equation (2.42) assumes the waveform is an up-chirp signal with the frequency linearly increasing as time increases. Also, this equation assumes that the pulse width equals

the Pulse Repetition Interval (PRI). The inverse of the PRF, the PRI determines how much time elapses between successive transmitted radar pulses. Setting the pulse width T equal to the PRI creates a Continuous-Wave (CW) signal. The CW signal has no impact on LFM simulation results and all it does is allow for more synthetic aperture array locations along the synthetic aperture than would a pulsed SAR. There are more range profiles and, therefore, more individual images to use in the imaging algorithm to produce a final image. The LFM waveform is a CW signal in order to match waveforms in future chapters.

The chirp rate α defines the slope of the linearly increasing frequency and depends on bandwidth and pulse-width. Determining this chirp rate requires knowledge of the phase and frequency maximum and minimum. The phase of this transmitted signal is

$$\phi = (f_c - B/2)t + \alpha t^2. \tag{2.43}$$

Taking the derivative of the phase results in frequency given by

$$\frac{\phi}{dt} = f_c - B/2 + 2\alpha t. \tag{2.44}$$

The extents (minimum and maximum) of the signal's frequency determine the bandwidth. The minimum and maximum expressions for the frequency are

$$\left[\frac{\phi}{dt}\right]_{\min,t=0} = f_c - B/2 \tag{2.45}$$

and

$$\left[\frac{\phi}{dt}\right]_{\max,t=T} = f_c - B/2 + 2\alpha T. \tag{2.46}$$

Subtracting the maximum from the minimum frequency equals the bandwidth. Performing this subtraction results in

$$\begin{aligned} B &= \left[\frac{\phi}{dt}\right]_{\max,t=T} - \left[\frac{\phi}{dt}\right]_{\min,t=0} && (2.47)\\ &= f_c - B/2 + 2\alpha T - (f_c - B/2) && (2.48)\\ &= 2\alpha T. && (2.49) \end{aligned}$$

Solving for the chirp rate α gives

$$\alpha = \frac{B}{2T}. \tag{2.50}$$

The bandwidth B and pulse width T determine the chirp rate. This relationship makes intuitive sense since the chirp rate is the rate of frequency change over the pulse width duration for the linearly increasing frequency. Using the values for bandwidth and pulse width for the scenario under considerion, the chirp rate becomes

$$\begin{aligned} \alpha &= \frac{20 \text{ MHz}}{2 \cdot \ 500 \ \mu\text{sec}} && (2.51)\\ \alpha &= 2.0 \text{ x } 10^{10} \ \frac{\text{cycles}}{\text{sec}^2}. && (2.52) \end{aligned}$$

In this research, two validation methods help characterize waveforms's effectiveness. One method involves the Ambiguity Function (AF) and the other involves frequency analysis of the transmitted waveform.

The AF examines all applicable Doppler frequencies and time delays possible for a given waveform. Mathematically, the AF is the magnitude squared of the matched filter output for all Doppler shifts and time delays [11]. This analysis is particularly important when investigating Doppler aliasing reduction. AFs show the nulls, or zero locations, at the proper locations to suppress Doppler aliasing. Using an LFM upchirp transmitted signal given by (2.42), Fig. 2.6 shows the resultant familiar AF for an LFM signal [11].

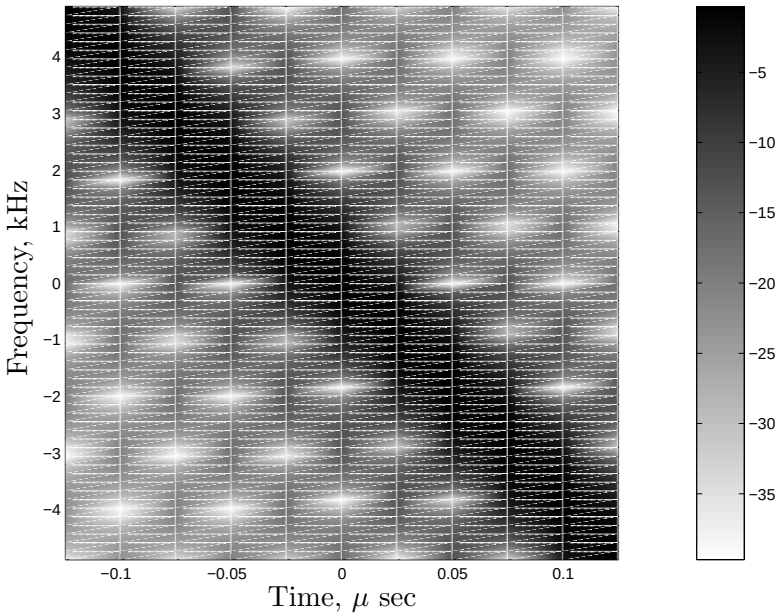

Figure 2.6: Ambiguity Function for LFM Waveform. Typical up-chirp LFM waveform AF exhibiting range-Doppler coupling. This coupling means that a time delay in a radar return could incorrectly place the scatterer in Doppler and vice versa.

The other validation tool involves frequency analysis on the waveform to ensure uniform bandwidth coverage. Uniform bandwidth coverage is essential for achieving good range resolution [11]. If there are any gaps in spectral coverage, then the analysis breaks down because of missing information. In this SAR scenario, the ideal case for frequency coverage is the LFM scenario as seen in Fig. 2.7. The other waveforms in this research attempt to have bandwidth coverage similar to the LFM waveform.

As the transmitted signal propagates outward from the radar, scatterers reflect the signal inducing a time delay and Doppler frequency shift that modify the transmitted signal. This modification results in a received signal written as

$$r(t) = \sum_{k=1}^{9} s(t - T_k) e^{[j2\pi f_k (t - T_k)]} \tag{2.53}$$

where T_k is the time delay and f_k is the Doppler frequency shift of the return signal of the k^{th} scatterer. Using this definition for a received signal, the simulation builds,

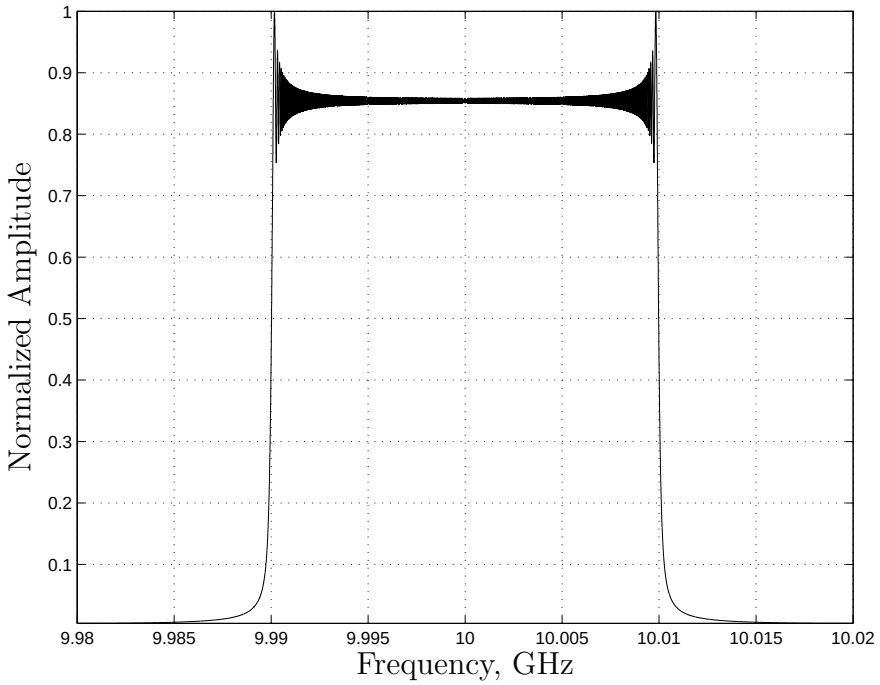

Figure 2.7: LFM Frequency Coverage. The bandwidth of $f_c - B/2 < f < f_c + B/2$ possesses uniform frequency coverage. RSF waveforms attempt to mimic this uniform coverage.

for each synthetic aperture location, a composite received signal that incorporates the received signals from each scatterer in the scene. The simulation then match filters the composite signal to produce a range profile. A final image forms by implementing the Back-Projection algorithm. The next section describes the results from using the LFM waveform in the WA-SAR scenario and the resulting effect of Doppler aliasing.

2.5.2 Results. Figure 2.8 shows the range profile from one synthetic aperture location (-100 m,0). The nine spikes correspond to the nine scatterers within the scene with the reference scatterer at the zero range position. This figure is only one of the range profiles from the entire synthetic aperture array. Although it shows magnitude, this range profile does not show the important phase information which is vital towards image formation. The range profile does validate the range information while the imaging process validates correct phasing in the returned signals.

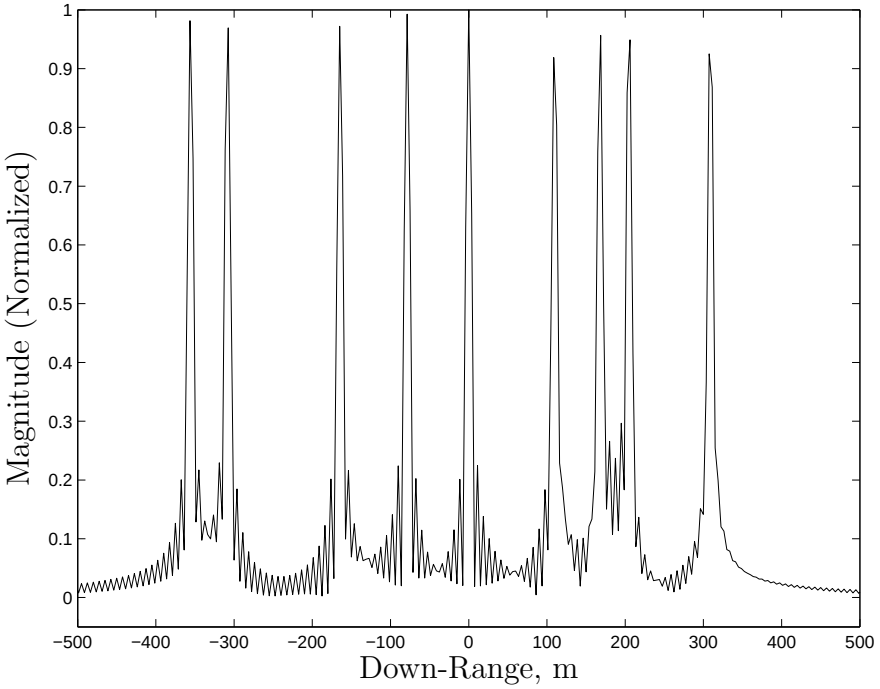

Figure 2.8: SAR Range Profile – LFM Waveform. This figure shows nine distinct scatterers from one range profile with the reference scatterer at 0 meters. Along with the other range profiles in the thesis, this figure shows a zoomed-in portion of the entire range profile defined by R_{min} to $R_{max} + cT/2$. The extent of the range profile corresponds to the down-range terrain patch image extent of 1000 m.

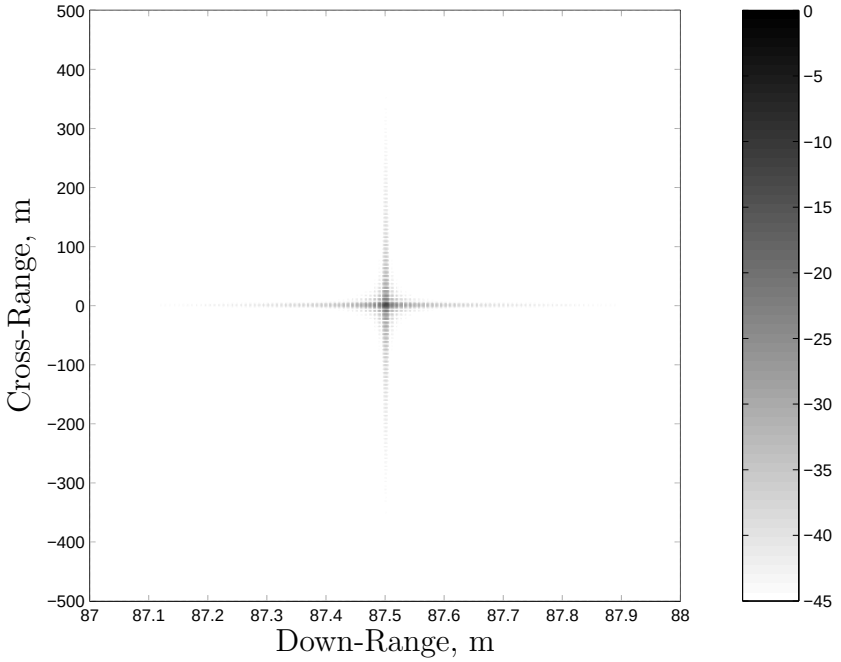

Figure 2.9: This figure shows the ideal image with a −45 dB dynamic range resulting from only having the reference scatterer in the scene. There are no effects of Doppler aliasing evident in this image. By comparing this image to other images, the effects of Doppler aliasing are evident.

For comparison purposes, Fig. 2.9 represents an ideal image of the simulation scene. It is important to see what the image would look like if no Doppler aliasing occurs. The image is ideal because the scene only contains the reference scatterer. The simulation removes all other scatterers to generate this image. This reference, baseline, image serves as a comparison tool for images produced by other waveforms in this research. Through this comparison, the effects of Doppler aliasing are clearly evident.

Figure 2.10(a) shows the effects of Doppler aliasing when using an LFM waveform in the WA-SAR scenario at a platform velocity of 100 m/s. The SAR image displays the expected results (cross-shaped sidelobe) for the scatterer of interest at its true location in range and cross-range (87.5 km, 0 m). The aliased scatterers, appearing trapezoidal in the image, are numbers 1, 3, 7, and 9 which correspond to those

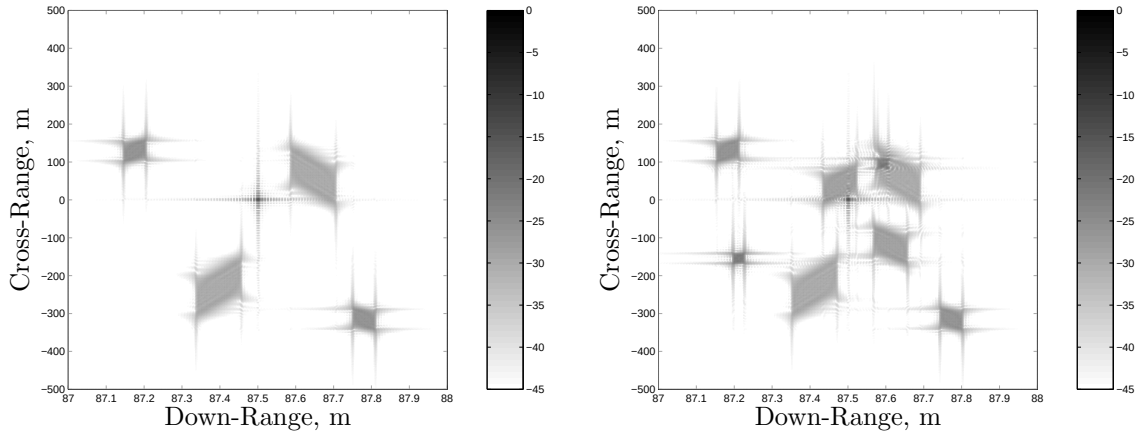

(a) (b)

Figure 2.10: (a) LFM Image at a platform velocity of 100 m/s with a −45 dB dynamic range. The scatterers that alias into the image have a Doppler frequency shift equal to an integer multiple of the PRF. Four scatterers alias into the image. (b) LFM Image at a platform velocity of 200 m/s with a −45 dB dynamic range. All remaining scatterers alias into the image in this case.

scatterers that have Doppler shifts that are integer multiples of the PRF. Table 2.3 illustrates that the aliased scatterers do possess Doppler frequency shifts at multiples of the PRF. These scatterers are not actually located in the range extents of the image. Therefore, the aliased scatterers appear trapezoidal because the Back-Projection algorithm is not able to correctly resolve these scatterers.

Figure 2.10(b) depicts the Doppler aliasing in the image when using an LFM waveform and platform velocity of 200 m/s. From Table 2.3, it is evident all of the scatterers in the scene alias into the image at a platform velocity of 200 m/s.

2.6 Summary

Chapter 2 explains topics ranging from SAR basics to generating images using LFM waveforms and the Back-Projection imaging algorithm. Before moving on to the next chapter, it is important to review previous results from LFM waveforms and to look forward to the next chapters. Figures 2.10(a) and 2.10(b) show the effects of Doppler aliasing when using an LFM waveform in the WA-SAR scenario. Doppler

aliasing occurs because the PRF does not meet the lower bound set by the Doppler bandwidth. In the forthcoming chapters, with the same lower bound violation, new waveforms exhibit properties that remove Doppler aliasing effects from these SAR images.

III. Doppler Aliasing Removal Using RSF Waveforms

This chapter validates the research in [8] by verifying the effectiveness of continuous wave (CW) Random Stepped-Frequency (RSF) waveforms in eliminating Doppler aliasing in Wide-Angle SAR (WA-SAR) images. Doppler aliasing results from widening the antenna beamwidth in this WA-SAR scenario without satisfying the Pulse Repetition Frequency (PRF) synthetic aperture sampling requirement. Given the correct setup, CW RSF waveforms remove this aliasing. The subpulse's frequency content in this waveform is uniform (fixed) across the duration of the subpulse. Chapters 4 and 5 discuss methods that attempt to enhance results by replacing the fixed frequency with an Linear Frequency Modulation (LFM) chirp across the subpulse.

3.1 Concept

The goal of this SAR technique is to produce high resolution alias-reduced images of a particular scatterer. A well-known method to produce high resolution images is to employ spotlight mode SAR [2,13]. However, spotlight mode confines the possibilities of high resolution images to a relatively small terrain patch size. Spotlight mode trades coverage area for the high resolution images. A method to enlarge the coverage area is to employ WA-SAR. In this analysis, WA-SAR increases the radar transmit beamwidth ($\Delta\phi \cong 90^o$) while operating in stripmap mode. SAR processing can adaptively focus on particular terrain patches in the scene as the platform flies linearly along the synthetic aperture.

There are several advantages afforded by WA-SAR. Provided the scatterer remains in the wide-angle beamwidth throughout L, the SAR system has the ability to choose which scatterer to focus on. SAR processing can adaptively focus on any scatterer at any range or Doppler frequency shift. Operationally, this advantage provides flexibility in choosing terrain patches to image. Another advantage of this approach is the scatterer remains in the radar beam for a longer time duration. This increase leads to an increase in image resolution.

While widening the radar beamwidth has advantages, there is a considerable drawback. Along with increasing radar's beamwidth, the Doppler bandwidth of the received radar echoes also increases. With an increase in Doppler bandwidth, the PRF requires a minimum increase through [2]

$$\text{PRF} \geqslant \frac{4v_a \sin(\Delta\phi/2)}{\lambda} \tag{3.1}$$

where v_a is the platform velocity, $\Delta\phi$ is the angular antenna beamwidth, and λ is the carrier signal's wavelength. The right-hand side of (3.1) represents the Doppler bandwidth of an echo signal. This equation is valid only for a broadside collection while in stripmap mode and assumes there are no strong scatterers in the sidelobes [2, 8]. If desiring to improve image resolution in SAR by increasing beamwidth, (3.1) requires a minimum increase in PRF to match the Doppler bandwidth. If the PRF cannot meet this minimum increase, undersampling occurs in the synthetic aperture resulting in Doppler aliasing. The increase in PRF may become too cumbersome to employ in an operational SAR system. Tradeoffs then occur between Doppler aliasing and radar beamwidth. By definition, WA-SAR requires a broad angular antenna beamwidth. which cannot change. Therefore, the SAR system must accept Doppler aliasing and mitigate its effects.

To suppress Doppler aliasing, WA-SAR needs to know the aliasing location in frequency. From radar theory, Doppler aliasing in frequency occurs at integer multiples of the PRF [11]. Aliasing mitigation in WA-SAR can use this fact to remove the aliasing. In [8], the technique to remove suppress this aliasing in WA-SAR is to employ a CW RSF waveform.

A basic stepped-frequency, or frequency-hopping, waveform is a signal that breaks up the pulse width in time with a different frequency across each subpulse. Basic here means the subpulse's frequency is uniform or fixed across the subpulse. Chapters 4 and 5 discuss applying a linearly increasing frequency across the duration of the subpulse.

With basic stepped-frequency waveforms, there are N distinct subpulses that divide the pulse width T into N separate pieces of T/N duration. If the system utilizes a bandwidth B, each subpulse has N different frequencies to choose from with each frequency separated by B/N. Stepped-frequency waveforms can imitate Linear Frequency Modulated (LFM) signals by linearly ordering the subpulse frequencies. This waveform is a discrete approximation to LFM, but would result in an ambiguity region similar to the continuous LFM Ambiguity Function (AF) diagram.

Although stepped-frequency waveforms do not require specific subpulse frequency ordering, there are advantages to specifying a subpulse frequency order. Specifically, Costas codes apply a predetermined ordering to the subpulse frequencies to achieve reduction in sidelobe levels [11]. The predetermined order in Costas codes reduces the height of range and Doppler sidelobe levels in the AF. Since the subpulse frequency order of Costas codes stay the same on a pulse-by-pulse basis, they only fill specific blocks with each pulse in the region of Fig. 3.1.

If the subpulse frequency order changes randomly pulse-by-pulse, then the $B \times T$ region eventually completely fills as the SAR platform flies along the synthetic aperture. Pulse-by-pulse, in this WA-SAR scenario, means each synthetic aperture array location. For each array location, the subpulse order is a random selection of the N^2 available squares in the $B \times T$ region. As the SAR platform moves down the aperture, the random nature of frequency selection ultimately fills the $B \times T$ region. According to [11], random frequency selection in a stepped-frequency waveform represents a noise-like waveform which has an AF that represents a thumbtack [11]. As the $B \times T$ region fills more completely by successive RSF waveforms, the AF expression $|\chi(T_r, f_d)|^2$ for the set of waveforms approaches [8]

$$|\chi(T_r, f_d)|^2 = |\text{sinc}(BT_r)\text{sinc}(Tf_d)|^2, \tag{3.2}$$

where B is the system bandwidth, T_r is the range delay, T is the pulse width, and f_d is the Doppler frequency shift. Given that there are no range ambiguities to mitigate

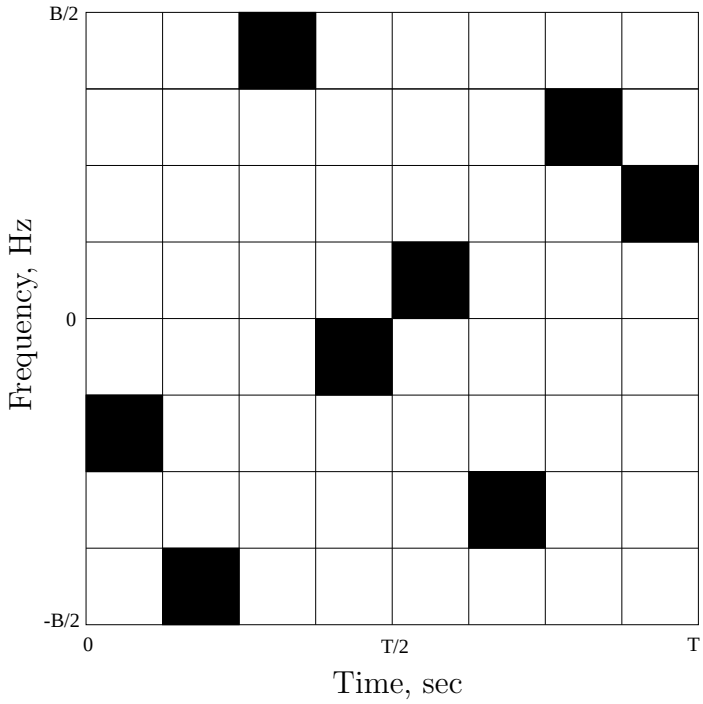

Figure 3.1: Time-Bandwidth Region for RSF waveforms ($N^2 = BT$). One example of a random subpulse ordering. The number of subpulses N equals 8 (illustration purposes only). In the simulation, the number of subpulses equals 100. Each synthetic aperture location randomly picks its own unique frequency ordering of subpulses and eventually completely fills the entire $B \times T$ region.

in this WA-SAR scenario, the primary focus of ambiguity reduction is on Doppler aliasing and, hence, the Doppler frequency factor $\text{sinc}(Tf_d)$ of (3.2).

Equation (3.2) has Doppler frequency nulls, or zeros, at non-zero integer multiples of $f_d = 1/T$. Remembering Doppler aliasing occurs at integer multiples of the PRF, the waveform uses these null locations at integer multiples of $1/T$ to remove Doppler aliasing. Specifically, if the pulse width T is set to

$$T = \frac{1}{\text{PRF}}, \tag{3.3}$$

the nulls of $\text{sinc}(Tf_d)$ coincide with the locations of the aliased scatterers. The AF then becomes

$$|\chi(T_r, f_d)|^2 = |\text{sinc}(BT_r)\text{sinc}(f_d/\text{PRF})|^2. \tag{3.4}$$

where the Doppler frequency nulls occur at nonzero integer multiples of the PRF. By setting T equal to 1/PRF, the Doppler frequency null location in the AF removes the Doppler aliasing dictating a CW waveform. This waveform is CW because setting T equal to 1/PRF corresponds to continuously transmitting a waveform throughout the synthetic aperture.

When attempting to focus on only one scatterer in WA-SAR, selecting a CW RSF waveform removes the scatterers that would otherwise alias into the image. Figure 3.2 shows the location of the nulls on the Doppler axis ($T_r = 0$) of the AF diagram.

The following paragraphs discuss the specifics of the WA-SAR scenario as it pertains to the waveform selection in this chapter. The paragraphs cover topics such as the number of subpulses and transmitted signal definition.

The number of subpulses in the waveform determine the number of partitions in the pulse width and frequency bandwidth. Normally, the time-bandwidth product of a radar waveform is $BT = 1$ [7]. However, a stepped-frequency waveform breaks the time into N subpulses. With a subpulse time duration at T/N and a frequency

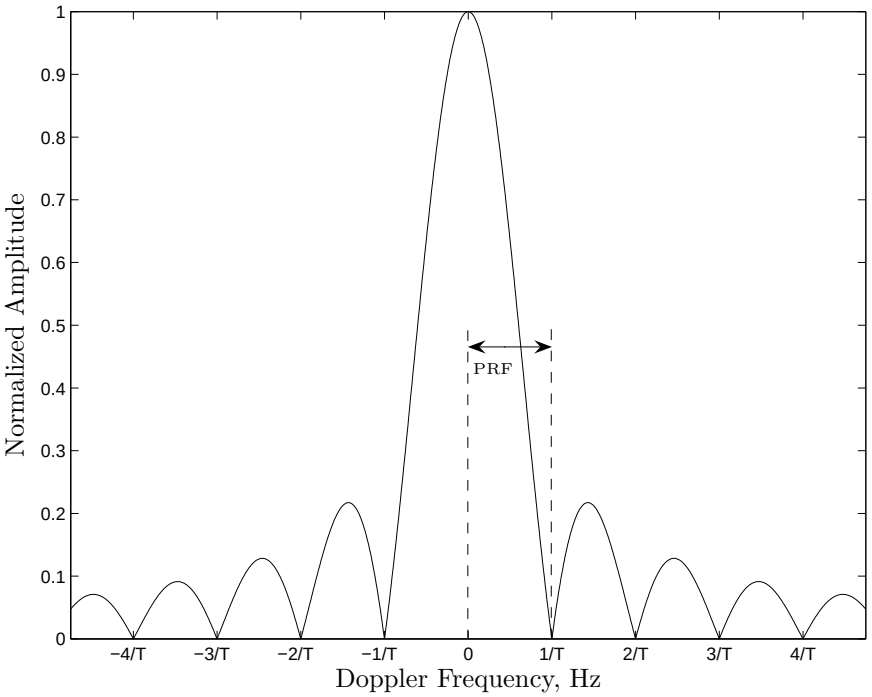

Figure 3.2: RSF Waveform Doppler Frequency Plot for $|\,[\mathrm{sinc}(f_d T) = \mathrm{sinc}(f_d/\mathrm{PRF})]\,|$. This plot is the $T_r = 0$ cut of the AF from (3.2).

spacing between bands at B/N, the number of subpulses is [11]

$$\begin{aligned} N &= \sqrt{BT} \\ &= \sqrt{20 \text{ MHz} \times 500 \ \mu\text{sec}} \\ &= 100 \end{aligned} \tag{3.5}$$

where B is the bandwidth of the system and T is the pulse width. Equation (3.5) refers to the time-bandwidth product for this chapter's waveform. With $N = 100$, there are 5 μsec in each subpulse and 200 kHz separating each subpulse frequency band. The relationship in (3.5) assures frequency coverage over every possible subpulse. Assuming a fixed carrier frequency across the subpulse and $N^2 < BT$, the frequency coverage of the waveform's subpulses do not fully cover the $B \times T$ region. If $N^2 > BT$, then the frequency coverage of individual subpulses expands too much for its required bandwidth. Chapter 4 retains the time-bandwidth product of (3.5) while replacing

the fixed frequency across the subpulse with an LFM chirp signal. This replacement attempts to increase Doppler aliasing supression by increasing frequency coverage in the $B \times T$ region. Chapter 5 attempts to violate (3.5) and change the time-bandwidth product to $BT > N^2$. Normally, this change would result in undesirable frequency overflow, but the frequency spacing between bands also changes to keep uniform bandwidth coverage for $f_c - B/2 < f < f_c + B/2$.

The following equation defines the transmitted CW RSF waveform:

$$s(t) = \sum_{\mathrm{i}=0}^{N-1} e^{j2\pi f_{\mathrm{i}} t} \qquad \mathrm{i}\frac{T}{N} < t < (\mathrm{i}+1)\frac{T}{N} \tag{3.6}$$

where N is the number of subpulses and f_{i} are the randomly selected subpulse frequencies between $f_c - B/2 < f_{\mathrm{i}} < f_c + B/2$ with each subpulse having a T/N time duration.

Definitions for the returned echo pulse, matched filter impulse response, and matched filter output remain the same as described in Chapter 2. The returned echo signal for the CW RSF waveform of a single scatterer is a time delayed and Doppler frequency shifted version of (3.6). The returned echo signal is then

$$r(t) = s(t - T_r)e^{[j2\pi f_d(t-T_r)]} \qquad T_r < t < T + T_r, \tag{3.7}$$

where T_r is the time delay, f_d is the Doppler frequency shift, and T is the pulse width. The matched filter impulse response is then

$$h(t) = \left\{ s(T_{\mathrm{rs}} - t)e^{[j2\pi f_{\mathrm{rs}}(T_{\mathrm{rs}}-t)]} \right\}^* \qquad T_{\mathrm{rs}} - T < t < T_{\mathrm{rs}}. \tag{3.8}$$

where T_{rs} is the reference scatterer time delay and f_{rs} is the reference scatterer Doppler frequency shift. The system output $y(t)$ is the convolution of received signal $r(t)$ with the matched filter impulse response $h(t)$ given by

$$y(t) = r(t) \otimes h(t). \tag{3.9}$$

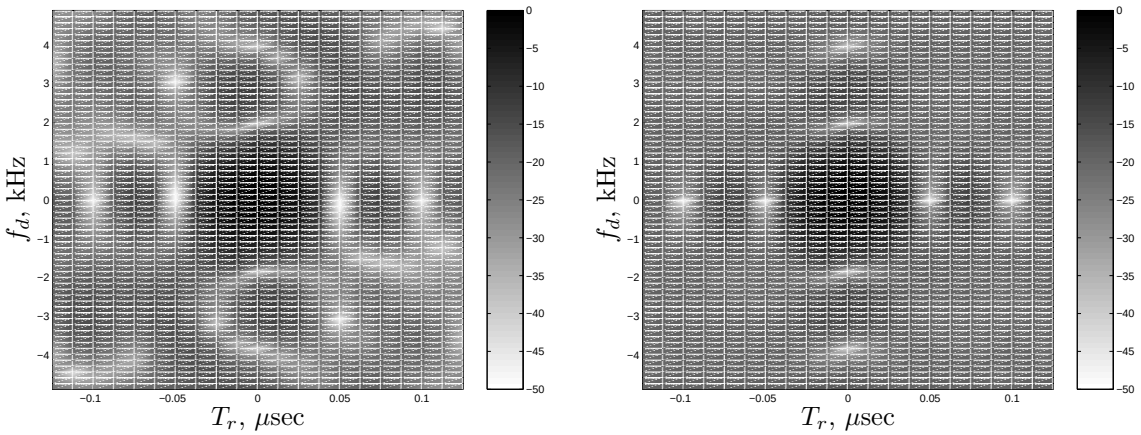

(a) (b)

Figure 3.3: (a) Ambiguity Function for One Realization of an RSF Waveform. This figure shows the noise-like Ambiguity Function for one RSF waveform [11].
(b) Ambiguity Function for 100 Realizations of RSF Waveforms. The set of RSF waveforms better approximate (3.2). Null location is correct at integer multiples of the PRF (2 KHz) and the ambiguity shape is similar to a 2-D sinc.

Image formation occurs via Back-Projection from processing the individual range profiles from each synthetic aperture location generated from (3.9). Back-Projection forms the final image by summing the individual images from the range profiles.

The AF for this waveform provides insight into its effectiveness at mitigating Doppler aliasing. Referring to Fig. 3.1, one realization of the RSF waveform fills only N of the possible N^2 squares in the $B \times T$ region. Therefore, one realization of the waveform does not provide an AF consistent with (3.2). Figure 3.3(a) shows the AF diagram for one realization of the RSF waveform which has nulls at nonzero integer multiples of $1/B = 0.05$ μsec and $1/T = 2000$ Hz. However, the general 2-D sinc-like function dictated by (3.2) is present only in a general sense.

By increasing the number of realizations, the $B \times T$ region in Fig. 3.1 fills more completely and the AF becomes a more appropriate approximation to (3.2). Figure 3.3(b) shows the distinct 2-D sinc structure and, most importantly, has the appropriate nulls at the integer multiples of the PRF (2000 Hz) on the Doppler fre-

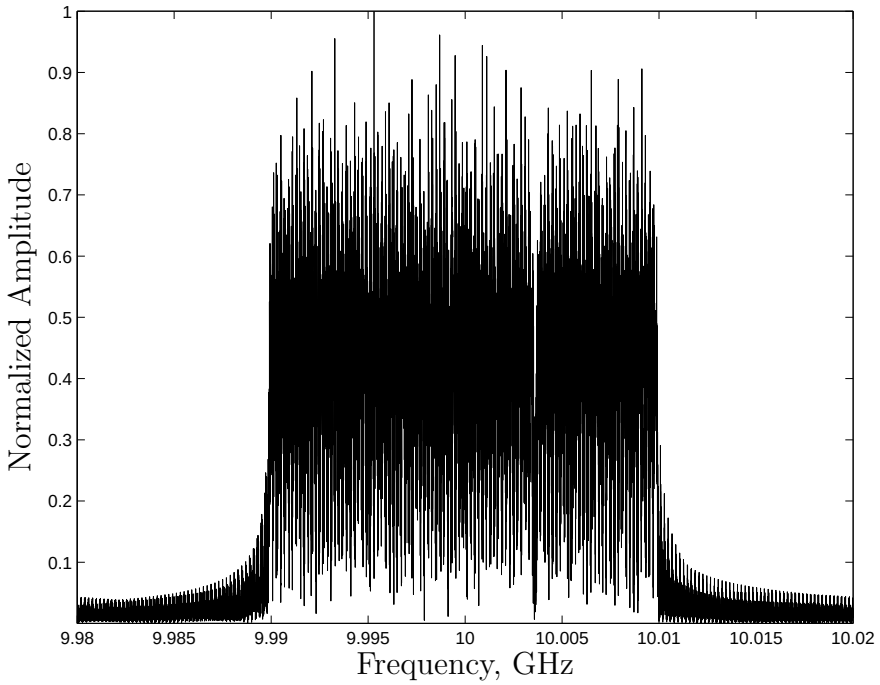

Figure 3.4: RSF Waveform Frequency Coverage for one range profile. No major gaps occur in the passband from $f_c - B/2 < f < f_c + B/2$ ensuring adequate frequency coverage.

quency axis. The null locations in this figure predict suppression of aliased scatterers due to Doppler aliasing.

Uniform frequency coverage is essential to attain theoretical range resolution and to ensure the range profile contains no range aliasing [11]. Hence, it is important to verify that a RSF waveform possesses uniform frequency coverage across the system passband $f_c - B/2 < f < f_c + B/2$ of the system. Referring to Fig. 3.4, this figure shows the RSF waveform exhibiting adequate frequency coverage over the passband. Frequency coverage is not completely uniform like in LFM waveforms, but there are no major gaps in RSF waveform frequency coverage in the passband.

3.2 Results

Through range profiles and SAR images, this section shows the effectiveness of the CW RSF waveform in removing WA-SAR Doppler aliasing.

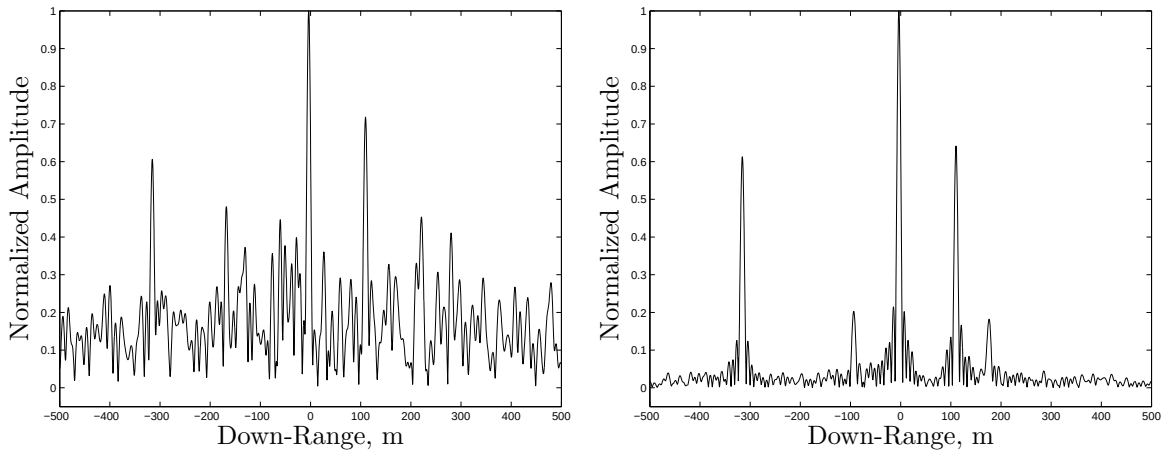

(a) (b)

Figure 3.5: (a) Range profile of one realization of RSF waveform at a platform velocity at 100 m/s. Noise from the single RSF waveform dominates much of the profile with scatterers 4 and 6 rising just above the noise floor because their Doppler shift is $f_d = \text{PRF}/2$.
(b) Range profile with 100 realizations. The noise floor does not dominate the range profile when compared to (a) because of the more structured nature of sets of RSF waveforms. Scatterers 4 and 6 are clearly visible in this figure because their Doppler shift is $f_d = \text{PRF}/2$.

3.2.1 Range Profile. Figure 3.5(a) shows one realization of the range profile (matched filter output) from one synthetic aperture array location. Equation 3.9 produces the output shown in this figure. One realization of the RSF waveform fills up N of the possible N^2 squares in the $B \times T$ region given in Fig. 3.1. Figure 3.5(a) shows the reference scatterer at the correct down-range location with a relatively high noise floor due to the noise-like AF of a single RSF waveform [11]. Noise is not added to the simulation model. Again, the noise floor relates to the noise-like AF of a single RSF waveform.

When the number of realizations of one range profile increases to 100, this set of random realizations of the RSF waveform improves the AF approximation in (3.2). With more realizations, the $B \times T$ region in Fig. 3.1 fills more uniformly. It is this filling of the $B \times T$ region that Chapters 4 and 5 attempt to improve upon.

Considering the choices of frequencies in Fig. 3.1 are random, there is no way to assure completely filling all N^2 squares, but 100 random realizations of a RSF waveform is appropriate since $N = 100$.

After 100 realizations of the CW RSF waveform, the reference scatterer in Fig. 3.5(b) is still at its proper location and magnitude, but the noise floor level decreases due to the better approximation of the AF. With this improving approximation, the function $\text{sinc}(f_d T)$ turns out to attenuate the scatterers in the range profile [8]. With nulls at integer multiples of the PRF, this function suppresses all scatterers with these attributes from the range profile. Referring to Table 3.1, scatterers 4 and 6 are clearly present in Fig. 3.5(b) since their Doppler frequency is $f_d = \text{PRF}/2$.

Figure 3.2 shows that a Doppler frequency shift of half the PRF lies halfway between the peak of the sinc function and its first null. At $PRF/2$, the normalized amplitude is around 0.6 in value. Therefore, Doppler frequencies allow scatterers 4 and 6 into the range profile at this normalized amplitude value.

Figure 3.6(a) shows the range profile after just one realization with a platform velocity of 200 m/s. Similar to $v_a = 100$ m/s, this range profile correctly resolves the reference scatterer in range with full magnitude. The noise floor is present again as well due to one RSF waveform appearing noise-like. Doppler filtering attenuates the other scatterers. According to Table 3.1, all of the scatterers have Doppler frequency shifts at integer multiples of the PRF. Consequently, no other scatterers are present in the range profile after 100 realizations. Figure 3.6(b) exhibits the range profile after 100 realizations of the RSF waveform at a platform velocity of 200 m/s. Again, the uniform filling of the $B \times T$ region allows for a better approximation of (3.2). Figure 3.6(b) illustrates the relatively low noise floor and the absence of other scatterers due to their Doppler characteristics and (3.2).

3.2.2 SAR Image. The application of CW RSF waveforms in the SAR research scenario result in a SAR image containing only the scatterer of interest at

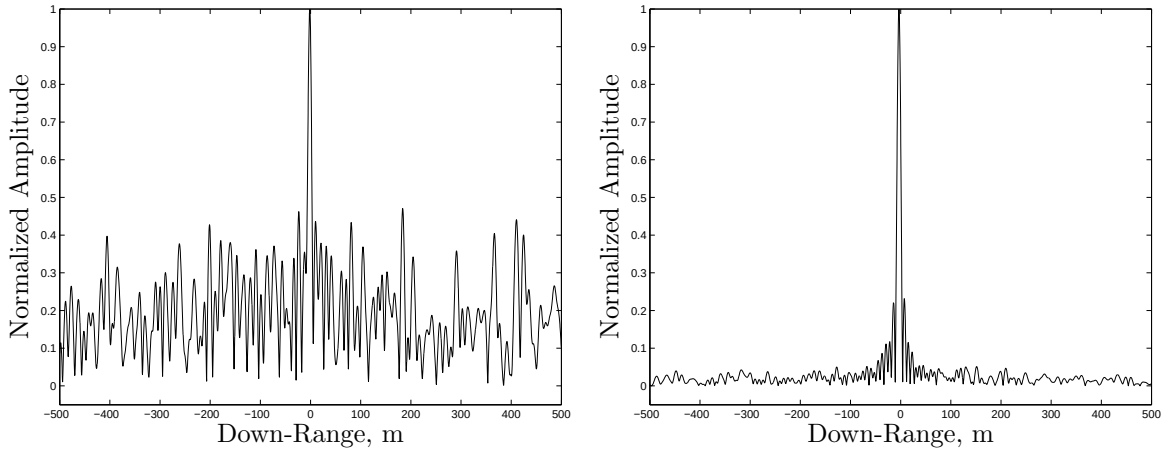

(a) (b)

Figure 3.6: (a) Range profile of one realization of RSF waveform at a platform velocity at 200 m/s. Noise from a single RSF waveform dominates much of the profile with no scatterers rising above the noise floor because no scatterers possess Doppler shifts of half the PRF.
(b) Range profile with 100 realizations. The noise floor does not dominate the range profile when compared to (a) because of the more structured nature of sets of RSF waveforms. No other scatterers enter the range profile.

Table 3.1: Scatterer Normalized Doppler Parameters

	Normalized Doppler ($\overline{\omega}$) (Hz)	
Scatterer	100 m/s	200 m/s
1	2.00	4.00
2	1.50	2.99
3	0.99	1.98
4	0.50	1.00
5	0	0
6	-0.51	-1.01
7	-1.00	-1.99
8	-1.50	-3.00
9	-2.01	-4.02

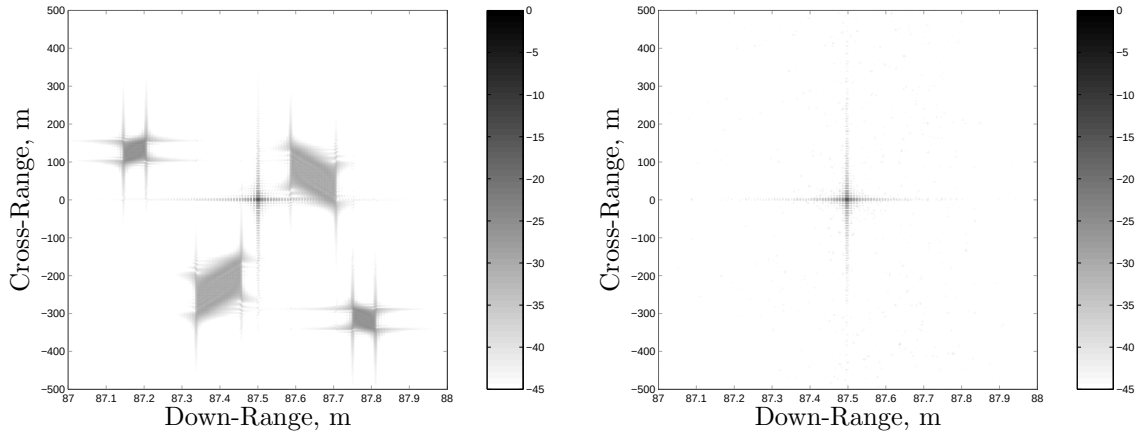

(a) (b)

Figure 3.7: (a) LFM Image at a platform velocity of 100 m/s with a −45 dB dynamic range. The scatterers that alias into the image have a Doppler frequency shift equal to an integer multiple of the PRF. 4 scatterers alias into the image in this case.
(b) RSF Image at a platform velocity of 100 m/s. The RSF waveform correctly images the scatterer of interest and removes the 4 aliased scatterers.

its true location in range and cross-range with associated noise floors. The waveforms remove Doppler aliasing seen in Figs. 3.7(a) and 3.8(a). The simulation uses the Back-Projection algorithm to process the range profiles into a final image. Figures 3.7(b) and 3.8(b) show the images at platform velocities of 100 and 200 ms/s respectively. These figures exhibit the removal of aliased scatterers from the LFM images and show a noise floor around −45 dB for $v_a = 100$ m/s and −40 dB for $v_a = 200$ m/s. The random nature of the set of RSF waveforms in the synthetic aperture virtually fills the $B \times T$ region in Fig. 3.1 to approximate (3.2). The waveform design effectively suppresses the scatterers at integer multiples of the PRF to result in alias-reduced SAR images.

According to [8], the noise floors in Figs. 3.7(b) and 3.8(b) result from two issues. The first issue is decorrelation between neighboring pulses due to varying range to the scatterers caused by the moving SAR platform. This decorrelation weakens the approximation of the RSF waveform AF given by (3.2) and reduces the depth of the

nulls at the aliased scatterer location. If there was no decorrelation, nulls at integer multiples of the PRF are theoretically at infinite depth. The nulls would then remove the aliased scatterers and noise floor completely from the image.

The other issue involves the aliased scatterers normalized Doppler characteristics. Referring to Table 3.1, aliased scatterers are not precisely at integer multiples of the PRF. Hence, the nulls at integer multiples of the PRF do not completely eliminate the aliased scatterers' energy content. Normalized Doppler frequencies are close enough to half the PRF to effectively remove the aliased scatterers.

Noise floor levels vary in the SAR images from -45 dB to -40 dB. The higher noise floor level at $v_a = 200$ m/s occurs because there are twice as many aliased scatterers to filter. With every other parameter staying constant, changing the platform speed decreases the number of pulses in the synthetic aperture. The decrease in pulses leads to fewer RSF waveforms to attempt to fill the $B \times T$ region in Fig. 3.1 which, therefore, weakens the approximation of the AF in (3.2). This weakening of (3.2) decreases null depth and contributes to a higher noise floor at $v_a = 200$ m/s.

3.3 Performance Metrics

Aliasing removal by the CW RSF waveforms is obvious through visual inspection of the images. However, it is important to quantitatively understand the amount of alias removal by this waveform. The following paragraphs discuss the thesis performance metric: Normalized Energy Reduction [8].

Regardless of waveform, the ideal imaging case is an image that contains only the scatterer of interest. Therefore, there is no opportunity for other scatterers to alias into the image. Figure 3.9 shows this ideal case. This figure *should* also represent the terrain patch of interest in the SAR scenario described in Chapter 2. The terrain patch of interest is 1000 m by 1000 m with the scatterer of interest in the center. This patch does not physically contain any of the other 8 scatterers. However, due to Doppler aliasing effects, some of the scatterers do enter the image. Hence, the

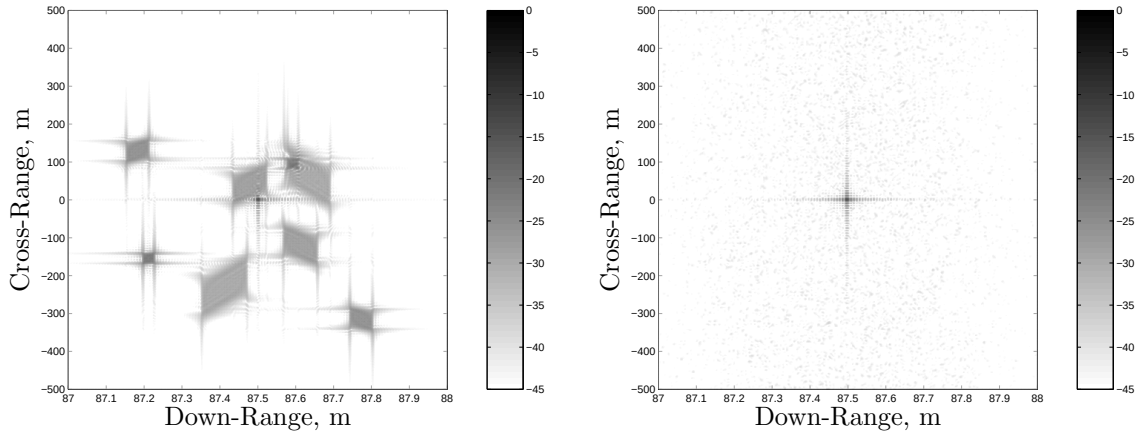

(a) (b)

Figure 3.8: (a) LFM Image at a platform velocity of 200 m/s with a −45 dB dynamic range. The scatterers that alias into the image have a Doppler frequency shift equal to an integer multiple of the PRF. All remaining scatterers alias into the image.
(b) RSF Image at a platform velocity of 200 m/s. The RSF waveform correctly images the scatterer of interest and removes the 8 aliased scatterers.

Table 3.2: Normalized Energy Summary.

	Normalized Energy Reduction (%)	
Waveform	100 m/s	200 m/s
RSF	98.99	93.46

energy in the terrain patch of the ideal case, Fig. 3.9, is the normalizing energy for the energy in other imaging cases. By summing the individual pixels, the energy in this ideal case is 1527. Normalized energy means dividing the energy from terrain patches of other waveforms by the energy from the ideal case. This measure assists in quantifying aliased energy removal. For example, the normalized energy for the ideal case is 1.00.

Referring to Fig. 3.7(a), the *normalized* energy from the LFM waveform at $v_a =$ 100 m/s is 1.456. This energy measure implies there is roughly 1.5 times the energy in the LFM scenario versus the ideal case. Implementing the CW RSF waveform results

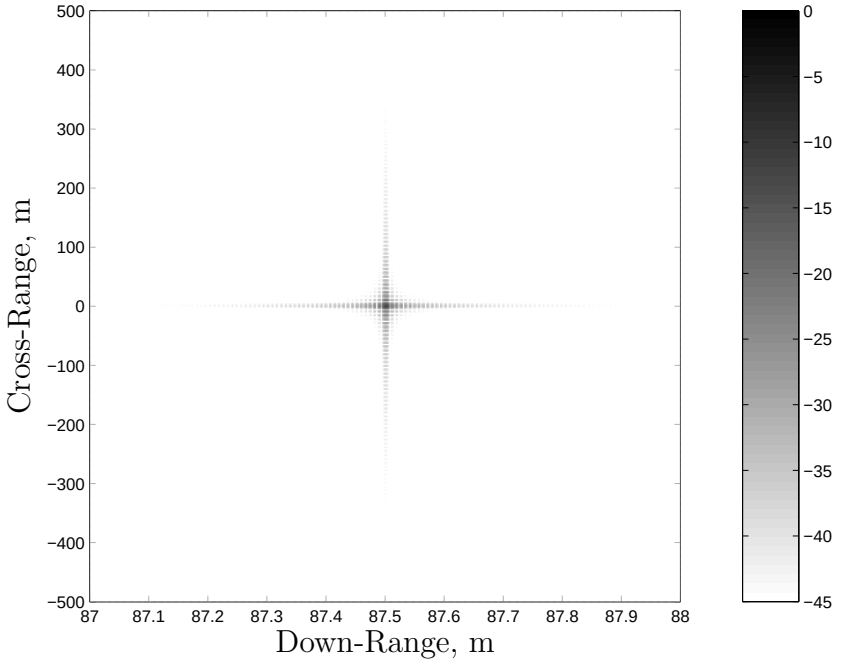

Figure 3.9: Ideal Image – Reference Scatterer. This figure shows the image with a −45 dB dynamic range resulting from only having the reference scatterer in the scene. There are no effects of Doppler aliasing evident in this image. By comparing this image to other images, the effects of Doppler aliasing are evident.

in a normalized energy of 1.005. As expected, this waveform significantly reduces the amount of aliased energy. The energy reduction is 98.99%. At $v_a = 200$ m/s, the LFM case results in a normalized energy of 1.764.

Compared to $v_a = 100$ m/s, Fig. 3.8(a) illustrates the additional energy introduced into the terrain patch due to the 4 extra aliased scatterers. The CW RSF waveform reduces normalized energy to 1.050, a 93.46 % reduction in aliased energy. Table 3.2 summarizes the normalized energy reduction.

3.4 Summary

This chapter shows that by implementing a CW RSF waveform in a WASAR system that alias-reduced image formation is possible. Doppler aliasing, shown in Figs. 3.7(a) and 3.8(a), results from the synthetic aperture undersampling the scene. The CW RSF images effectively suppress these aliased scatterers as seen in Figs. 3.7(b) and 3.8(b).

Implementation of this CW RSF waveform to remove Doppler aliasing is only possible by randomly selecting frequencies to fill up the $B \times T$ region of Fig 3.1. Chapters 4 and 5 attempt to improve the coverage in the $B \times T$ region by applying an LFM chirp to the subpulses.

IV. Doppler Aliasing Removal Using LFM-RSF Waveforms

This chapter describes Doppler aliasing reduction in Wide-Angle SAR (WA-SAR) by implementing a Continuous Wave (CW) Random Stepped-Frequency waveform (RSF) with Linear Frequency Modulated (LFM-RSF) chirp signals on the waveforms's subpulses. This analysis attempts to gain greater frequency coverage than in the previous chapter, thereby improving aliased scatterer suppression.

4.1 Concept

The scenario in this chapter is the same as in Chapter 3: obtain high resolution images using WA-SAR. In this chapter, LFM chirp signals replace the fixed frequency signals across the subpulses of the CW RSF waveform. By applying this waveform to the WA-SAR scenario, improvement in suppressing aliased scatterer energy is possible. All other system parameters and configurations remain unchanged from Chapter 3. The new transmitted LFM-RSF waveform is given by

$$s(t) = \sum_{\mathrm{i}=0}^{N-1} e^{\left[j2\pi(f_{\mathrm{i}}t+\alpha t^2)\right]} \qquad \mathrm{i}\frac{T}{N} < t < (\mathrm{i}+1)\frac{T}{N} \tag{4.1}$$

where N is the number of subpulses, f_{i} are the randomly selected subpulse frequencies between $f_c - B/2 < f_{\mathrm{i}} < f_c + B/2$ with each subpulse having a T/N time duration.

The motive for replacing the uniform frequency with LFM chirp signals across the subpulses of the CW RSF waveform is greater frequency coverage in the $B \times T$ data region. Figure 4.1 graphically shows the LFM chirp signals on each subpulse. Greater frequency coverage correlates to filling the $B \times T$ region more completely and improving the Ambiguity Function (AF) approximation for sets of RSF waveforms given by

$$|\chi(T_r, f_d)|^2 = |\mathrm{sinc}(BT_r)\mathrm{sinc}(Tf_d)|^2, \tag{4.2}$$

where B is the system bandwidth, T_r is the time delay, T is the pulse width, and f_d is the Doppler frequency shift. It is this enhanced approximation that deepens the Doppler frequency nulls in the AF at the aliased scatterers location (integer multiples

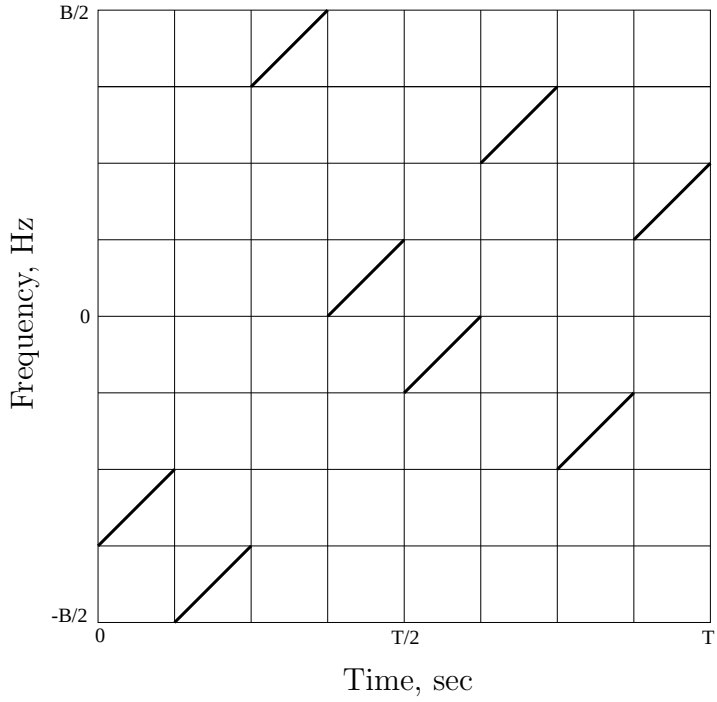

Figure 4.1: Time-Bandwidth region for LFM-RSF waveforms ($N^2 = BT$). One example of a random ordering of the subpulses. The number of subpulses N equals 8 (illustration purposes only). In the simulation, the number of subpulses equals 100. Each synthetic aperture location randomly picks its own unique LFM signal ordering of subpulses and eventually completely fills the $B \times T$ region. The diagonal lines in the figure represent the LFM up-chirp signals.

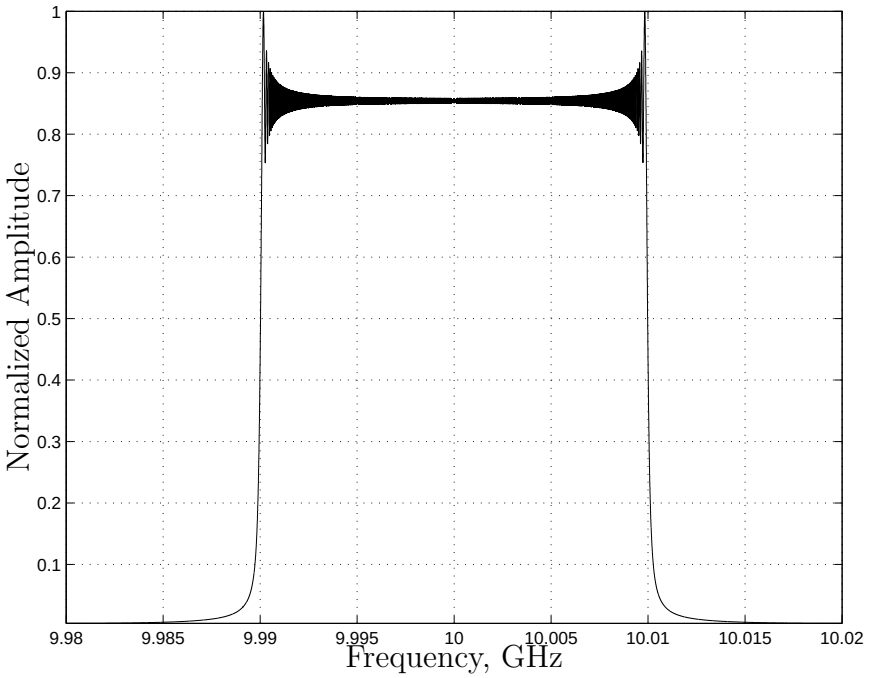

Figure 4.2: LFM Frequency Coverage. This waveform has uniform frequency coverage across its passband of $f_c - B/2 < f < f_c + B/2$. The subpulse frequency coverage should be similar to this figure. However, insufficient subpulse duration and bandwidth does not allow for improved frequency coverage over fixed frequency signals.

of the PRF). By increasing the null depth, this waveform increases the amount of aliased scatterer energy suppression.

The key to the enhanced AF approximation is the larger subpulse frequency coverage of an LFM chirp signal compared to a fixed frequency signal. Theoretically, the frequency coverage of a fixed frequency signal is sinc-like. Conversely, the frequency coverage of an LFM chirp signal is a "batwing" shape. Figure 4.2 shows the frequency coverage of an LFM signal across the full system bandwidth B and the entire pulse width T. Assuming constant bandwidth and pulse width, the LFM signal covers more frequency than a fixed frequency signal. This theoretical increase in frequency coverage fills the $B \times T$ region more completely which results in a better approximation of the AF in (4.2).

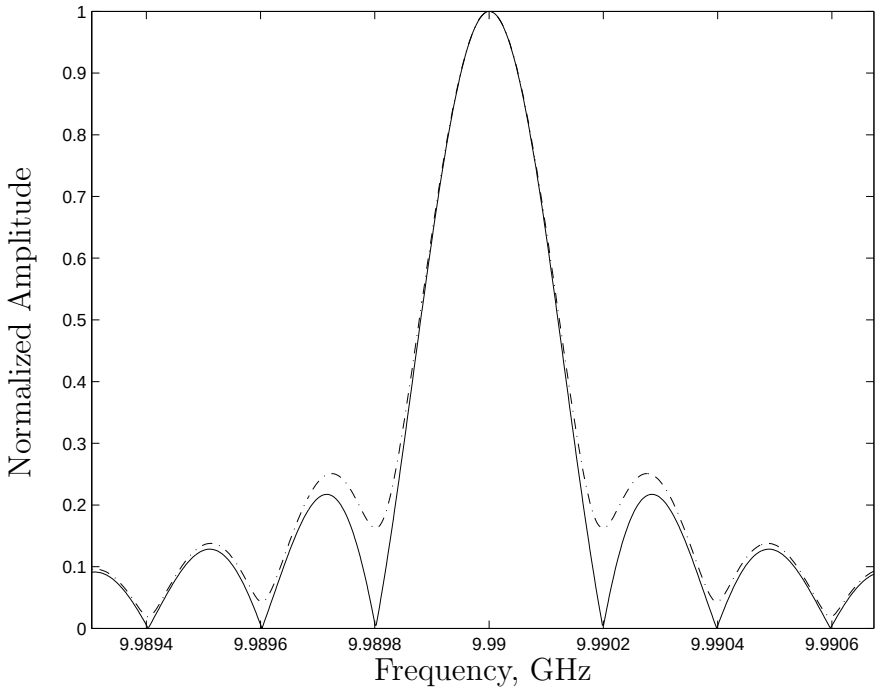

Figure 4.3: RSF waveform (solid) versus LFM-RSF waveform (dashed) frequency coverage. For a single subpulse, LFM-RSF waveforms covers slightly more frequency than RSF waveforms. Insufficient subpulse duration and bandwidth does not allow for improved frequency coverage over fixed frequency signals. This slight improvement in frequency coverage does not greatly enhance suppression of Doppler aliasing.

The actual frequency coverage from the LFM chirped subpulses ($BT = N^2$) is not a significant increase compared to the frequency coverage in a fixed frequency signal. The time duration of the subpulse T/N is too short to cause a large enough frequency change across the subpulse. The consequence of this small LFM chirp frequency spread is frequency coverage appearing more like a fixed frequency signal than an LFM chirp. The subpulse time duration, not frequency change, is the dominant cause of the spread in frequency. Referring to Fig. 4.3, the frequency coverage for the LFM chirp signal across the subpulse is only slightly larger than the fixed frequency signal frequency coverage. Chapter 5 discusses a method of reducing the number of subpulses to increase the spread of subpulse frequencies.

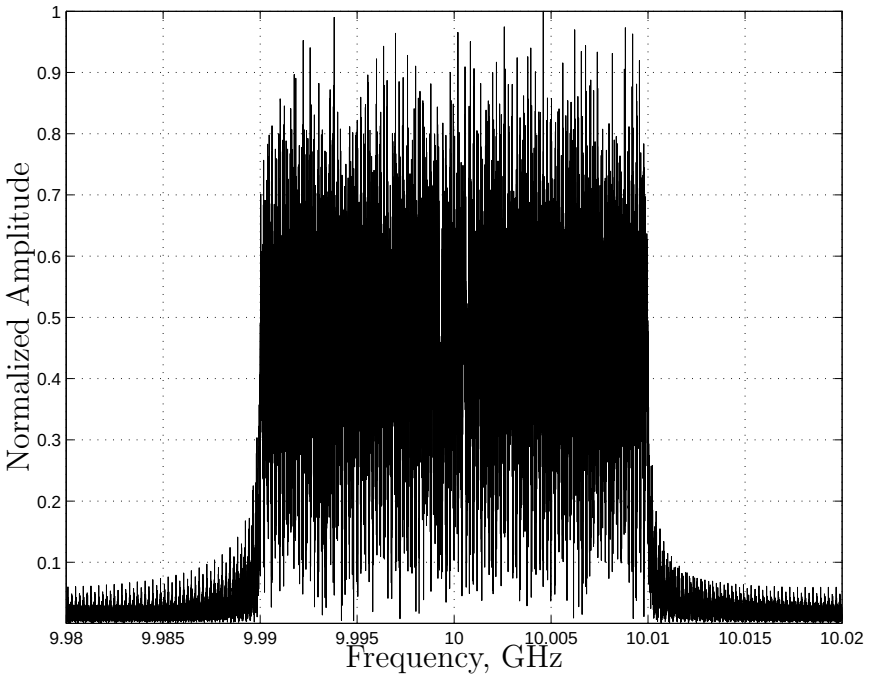

Figure 4.4: LFM-RSF Waveform Frequency Coverage for one range profile. No major gaps occur in the passband of $f_c - B/2 < f < f_c + B/2$ ensuring adequate frequency coverage.

Figure 4.4 shows the frequency coverage of one complete LFM-RSF waveform. (System bandwidth B remains unchanged throughout the research!) There are no gaps in the frequency coverage. This waveform achieves the required uniform frequency coverage across the bandwidth to achieve range resolution and reject range aliasing in the range profile [11].

The AF diagram for the transmitted signal in (4.1) exhibits similar characteristics as the AF diagrams from Chapter 3. Figure 4.5(a) shows the AF after one realization of a CW LFM-RSF waveform. This figure shows the the nulls at integer multiples of the PRF without the 2-D sinc shape as expected. Figure 4.5(b) shows the AF diagram after 100 realizations that better approximates the AF in (4.2). Again, this approximation improvement stems from filling the $B \times T$ region in Fig. 4.1 more uniformly.

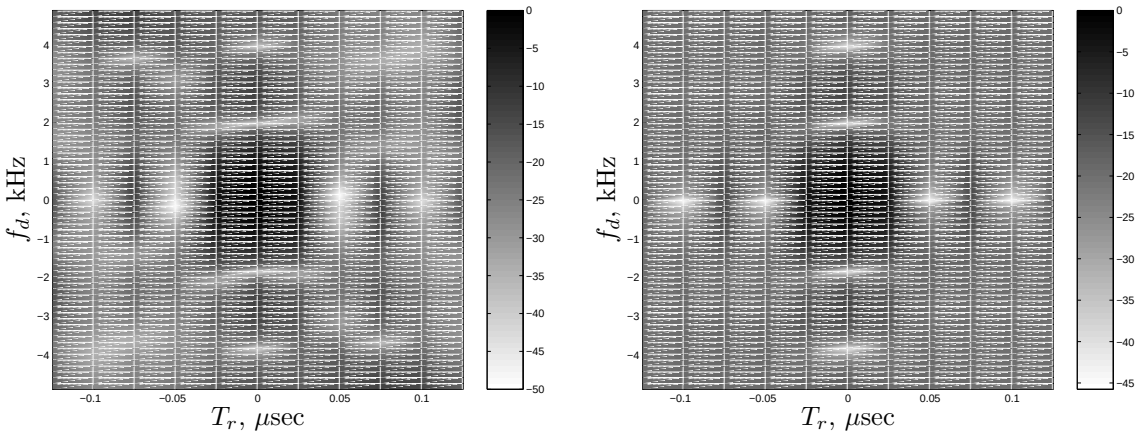

(a) (b)

Figure 4.5: (a) Ambiguity Function for One Realization of an LFM-RSF Waveform. This figure shows the noise-like Ambiguity Function for one LFM-RSF waveform [11]. (b) Ambiguity Function for 100 Realizations of LFM-RSF Waveforms. The set of LFM-RSF waveforms better approximate (4.2). Null location is correct at integer multiples of the PRF (2 KHz) and the ambiguity shape is similar to a 2-D sinc.

4.2 Results

Through range profiles and SAR images, this section shows the effectiveness of the CW LFM-RSF waveform in removing WA-SAR Doppler aliasing.

4.2.1 Range Profile. Figure 4.6(a) shows one realization of the range profile from one synthetic aperture array location at a platform velocity of 100 m/s. A single realization of the LFM-RSF waveform fills up N of the possible N^2 squares in the $B \times T$ region given in Fig. 4.1. This single realization results in a noise-like waveform with a thumbtack AF [11]. Figure 4.6(a) shows the reference scatterer at the correct down-range location with a relatively high noise floor due to this noise-like AF. When the number of realizations of one range profile increases to 100, the set of random realizations of the LFM-RSF waveform fills $B \times T$ region in Fig. 4.1 more uniformly and improves the approximation of the AF in (4.2). After 100 realizations of the CW LFM-RSF waveform, the reference scatterer in Fig. 4.6(b) is still at its proper location and magnitude, but the noise floor level decreases due to improved AF approximation.

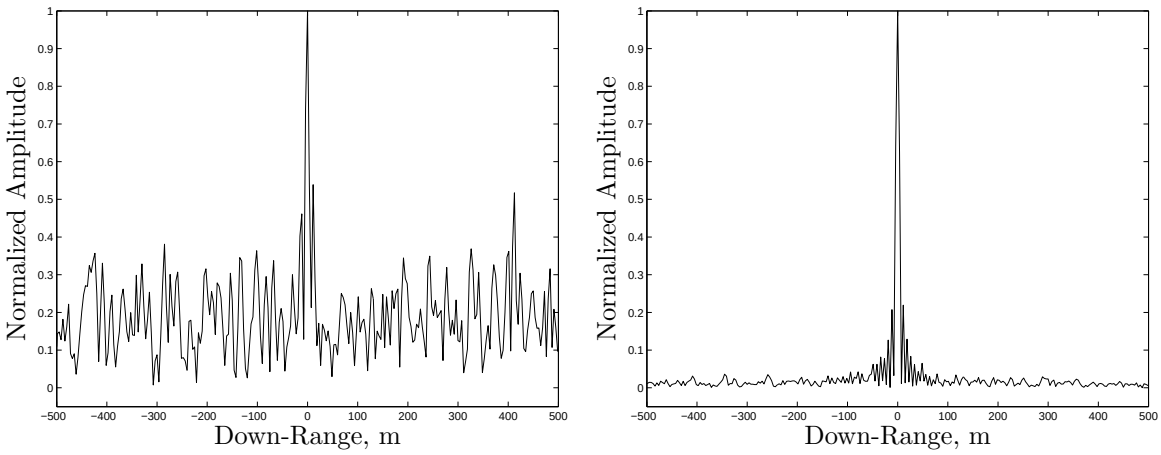

(a) (b)

Figure 4.6: (a) Range profile of one realization of LFM-RSF waveform at a platform velocity at 100 m/s. Noise from the single RSF waveform dominates much of the profile.
(b) Range profile with 100 realizations. The noise floor does not dominate the range profile when compared to (a) because of the more structured nature of sets of RSF waveforms.

Figure 4.7(a) shows the range profile after one realization of the waveform with a platform velocity of 200 m/s. Similar to $v_a = 100$ m/s, this range profile correctly resolves the reference scatterer in range with full magnitude. The noise floor is present again as expected. Figure 4.7(b) exhibits the range profile after 100 realizations of the LFM-RSF waveform. This figure illustrates the anticipated low noise floor and the absence of other scatterers due to their Doppler characteristics and (4.2).

4.2.2 SAR Image. The application of CW LFM-RSF waveforms in the SAR research scenario results in SAR images containing only the scatterer of interest at its true location in range and cross-range with associated noise floors. The waveforms reduce Doppler aliasing seen in Figs. 4.8(a) and 4.9(a). Image formation occurs via Back-Projection from processing the individual range profiles from each synthetic aperture location. Back-Projection forms the final image by summing the individual images from the range profiles. Figures 4.8(b) and 4.9(b) show the images at platform velocities of 100 and 200 ms/s respectively. Table 4.1 shows the expected scatterers

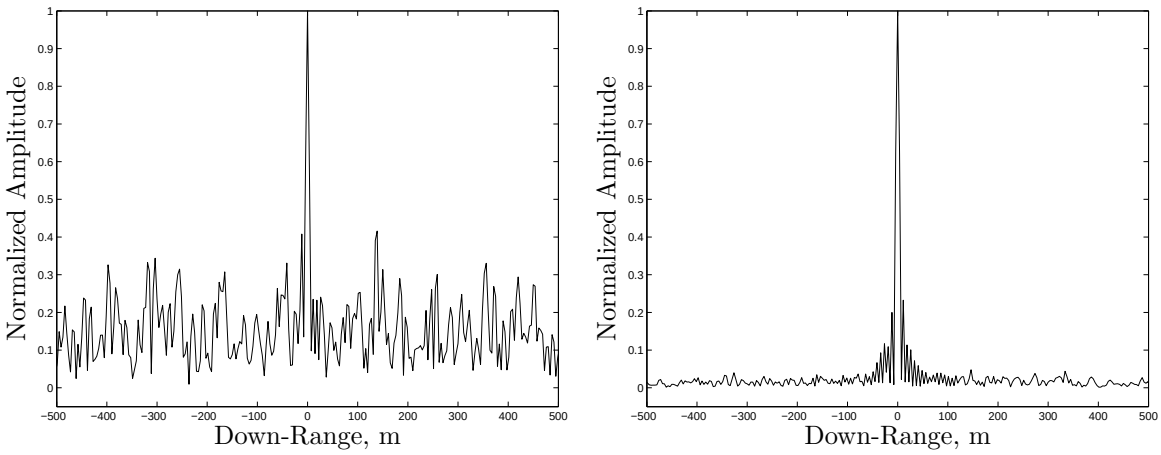

(a) (b)

Figure 4.7: (a) Range profile of one realization of LFM-RSF waveform at a platform velocity at 200 m/s. Noise from the single RSF waveform dominates much of the profile.
(b) Range profile with 100 realizations. The noise floor does not dominate the range profile when compared to (a) because of the more structured nature of sets of RSF waveforms.

that should alias into the SAR image at both platform velocities. These figures exhibit the suppression of aliased scatterers from the LFM images and a noise floor around -45 dB for $v_a = 100$ m/s and -40 dB for $v_a = 200$ m/s. Over the course of the synthetic aperture, the random nature of the set of LFM-RSF waveforms in the synthetic aperture virtually fills the $B \times T$ region in Fig. 4.1 to approximate (4.2). The waveform design effectively suppresses the scatterers at integer multiples of the PRF resulting in alias-reduced SAR images.

In Fig. 4.9(b), a noticeable mass of energy is visible on the Doppler axis ($T_r = 0$). This mass has a maximum dB magnitude of -22.24 corresponding to a 0.077 normalized magnitude. While it clouds a minor portion of the image, this energy mass's contribution to the overall energy value of the terrain patch is minimal at 0.077 per pixel.

Table 4.1: Scatterer Normalized Doppler Parameters

	Normalized Doppler ($\overline{\omega}$) (Hz)	
Scatterer	100 m/s	200 m/s
1	2.00	4.00
2	1.50	2.99
3	0.99	1.98
4	0.50	1.00
5	0	0
6	-0.51	-1.01
7	-1.00	-1.99
8	-1.50	-3.00
9	-2.01	-4.02

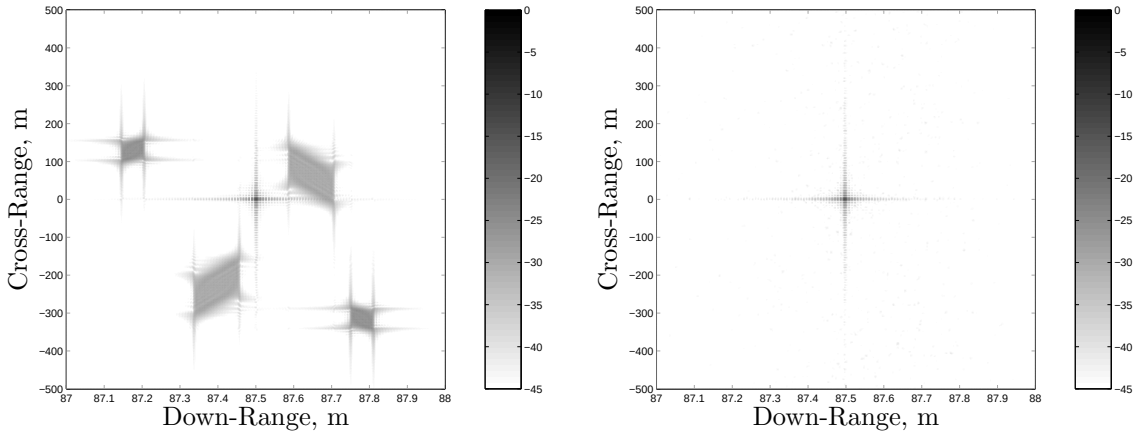

(a) (b)

Figure 4.8: (a) LFM Image at a platform velocity of 100 m/s with a -45 dB dynamic range. The scatterers that alias into the image have a Doppler frequency shift equal to an integer multiple of the PRF. 4 scatterers alias into the image in this case.
(b) LFM-RSF image at a platform velocity of 100 m/s. The LFM-RSF waveform correctly images the scatterer of interest and removes the 4 aliased scatterers.

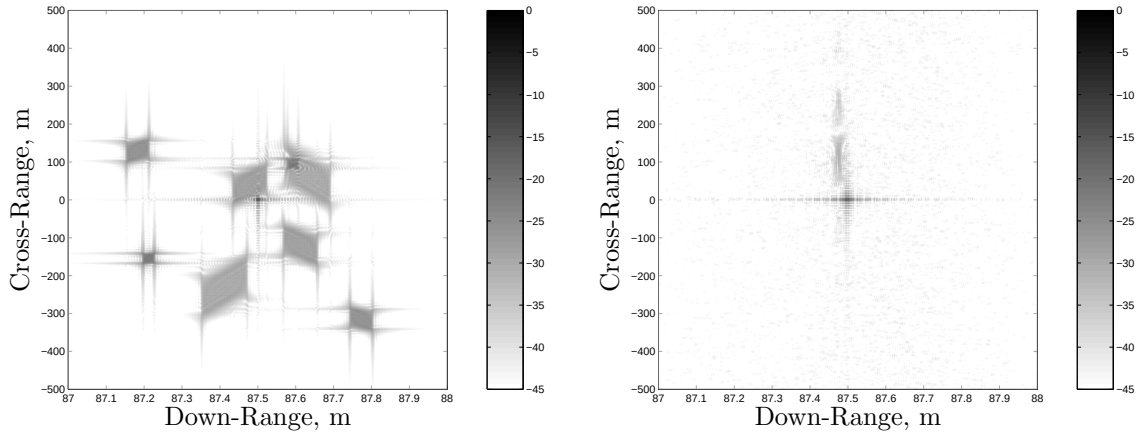

(a) (b)

Figure 4.9: (a) LFM Image at a platform velocity of 200 m/s with a −45 dB dynamic range. The scatterers that alias into the image have a Doppler frequency shift equal to an integer multiple of the PRF. All remaining scatterers alias into the image in this case.
(b) LFM-RSF image at a platform velocity of 200 m/s. The LFM-RSF waveform correctly images the scatterer of interest and removes the aliased scatterers.

4.3 Performance Metrics

Aliasing suppression by the CW LFM-RSF waveforms is obvious through visual inspection of the images. However, it is important to quantitatively understand the amount of alias reduction by this waveform.

Implementing the CW LFM-RSF waveform results in alias-reduced images. Referring to Fig. 4.8(a), the aliased scatterers are spread around the scatterer of interest in the image at $v_a = 100$ m/s. Figure 4.8(b) shows the image resulting from the implementation of the CW LFM-RSF waveform. The amount of normalized energy in this case is 1.002. This waveform significantly reduces the amount of aliased energy from the LFM case by 99.57%. With $v_a = 200$ m/s, Fig. 4.9(a) illustrates the additional energy introduced into the terrain patch image due to the 4 extra aliased scatterers. Figure. 4.9(b) shows that a CW LFM-RSF waveform removes all aliased scatterers. This waveform reduces normalized energy to 1.066: a 91.35% reduction in aliased energy. Table 4.2 summarizes the normalized energy reduction.

Table 4.2: Normalized Energy Summary.

	Normalized Energy Reduction (%)	
Waveform	100 m/s	200 m/s
RSF	98.99	93.46
LFM-RSF ($N^2 = BT$)	99.57	91.35

4.4 Summary

This chapter shows that implementing a CW LFM-RSF waveform in a WA-SAR system produces alias-reduced images. Chapter 5 attempts to improve the frequency coverage in the $B \times T$ data region attained in this chapter (refer to Fig 4.3) by reducing the amount of subpulses in the LFM-RSF waveform with a particular relationship between subpulse time duration and center-to-center subpulse frequency interval. This reduction in subpulses leads to a frequency coverage expected from an LFM signal.

V. Doppler Aliasing Removal Using Modified LFM-RSF Waveforms

This chapter discusses another waveform design to reduce Doppler aliasing in Wide-Angle SAR (WA-SAR). The waveform is still a Continuous Wave (CW) Random Stepped-Frequency waveform with Linear Frequency Modulated (LFM-RSF) chirp signals on the waveform's subpulses. The difference between this waveform and the waveform in Chapter 4 is fewer number of subpulses across the pulse width. By reducing the number of subpulses, the waveform attempts to gain greater frequency coverage than previous waveforms and suppress more aliased scatterer energy.

5.1 Concept

The scenario in this chapter is the same as in Chapters 3 and 4: obtain high resolution images by using WA-SAR. In this chapter, LFM chirp signals replace the fixed frequency signals across the subpulses of the CW RSF waveform. This waveform differs from the waveform in Chapter 4 by reducing the number of subpulses in order to gain greater frequency coverage. However, reducing subpulses does have drawbacks.

In general, the time-bandwidth product of a radar waveform is $BT = 1$ [7]. However, this equation needs modification because a RSF waveform breaks the pulse width into N subpulses. With a subpulse time duration of T/N and a center frequency difference between each subpulse of B/N, the time-bandwidth product is [11]

$$N^2 = BT, \tag{5.1}$$

where N is the number of subpulses, B is the system bandwidth, and T is the pulse width. This chapter attempts to increase frequency coverage for the individual subpulses by decreasing the number of subpulses N required by (5.1). With B at 20 MHz and T at 500 μsec, the number of required subpulses is 100. Decreasing the number

of subpulses in the waveform modifies (5.1) to become

$$N^2 < BT. \tag{5.2}$$

According to [7], a relationship exists between T/N and B/N permitting a reduction in N while maintaining the same bandwidth as a waveform with N subpulses.

From this point, the thesis establishes alternate expressions for T/N and B/N. The change in notion matches what is found in [7]. The subpulse time duration T/N changes to t_b. Also, the center frequency difference between each subpulse B/N changes to Δf. Hence, an alternate form of (5.1) is

$$t_b \Delta f = 1. \tag{5.3}$$

In [7], the authors describe a relationship between Δf, t_b, and B_s (bandwidth within each subpulse) authorizing a decrease in N subpulses while keeping the same bandwidth as an N subpulse RSF waveform. According to [6], this relationship allows a reduction in N because it removes the grating lobes in the autocorrelation function of Costas codes that occur when $\Delta f > 1/t_b$. A discussion on the applicability of Costas codes theory in this research is later in this chapter. The grating lobes occur at integer multiples of $1/\Delta f$. The relationship $\Delta f > 1/t_b$ implicitly prescribes a decrease in the number of required subpulses. The autocorrelation function is the zero Doppler axis ($|\chi(T_r, 0)|^2$) of the transmitted waveform's Ambiguity Function (AF). The autocorrelation function shows time axis behavior of a waveform. In this case, grating lobes are undesirable copies of the the main lobe across time in the autocorrelation function. The relationship between Δf and t_b allowing a decrease in N is [7]

$$t_b \Delta f = 5 \tag{5.4}$$

and

$$t_b B_s = 12.5. \tag{5.5}$$

Equations (5.4) and (5.5) remove the autocorrelation function grating lobes in Costas codes when decreasing N. Although Costas codes are used in [7], the waveforms in this research can also utilize the relationships in (5.4) and (5.5) because Costas codes are stepped-frequency waveforms themselves. The difference is the randomized selection of subpulse order with the waveforms in this research. Costas codes use a predetermined subpulse order. Consequently, the theory that developed the relationships in (5.4) and (5.5) is also applicable to the waveforms in this research.

Using (5.4) and (5.5), two relationships develop to determine the number of subpulses. The two relationships are

$$N = \frac{T\Delta f}{5} \tag{5.6}$$

and

$$N = \frac{TB_s}{12.5}. \tag{5.7}$$

Since N must be an integer and below the theoretical value from previous chapters (100), the number of subpulses chosen to satisfy the previous equations is 45. Hypothetically, any number that satisfies (5.4) and (5.5) can be chosen. Although, 45 subpulses lengthens the subpulse duration t_b giving the frequency enough time to linearly increase within t_b. Figure 5.1 shows the effect of reducing N to 45 subpulses. A later discussion in this chapter describes this frequency issue in more detail. The subpulse duration t_b is then

$$\begin{aligned} t_b &= \frac{T}{N} \\ t_b &= \frac{500\ \mu\text{sec}}{45} \\ t_b &= 11.11\ \mu\text{sec}. \end{aligned} \tag{5.8}$$

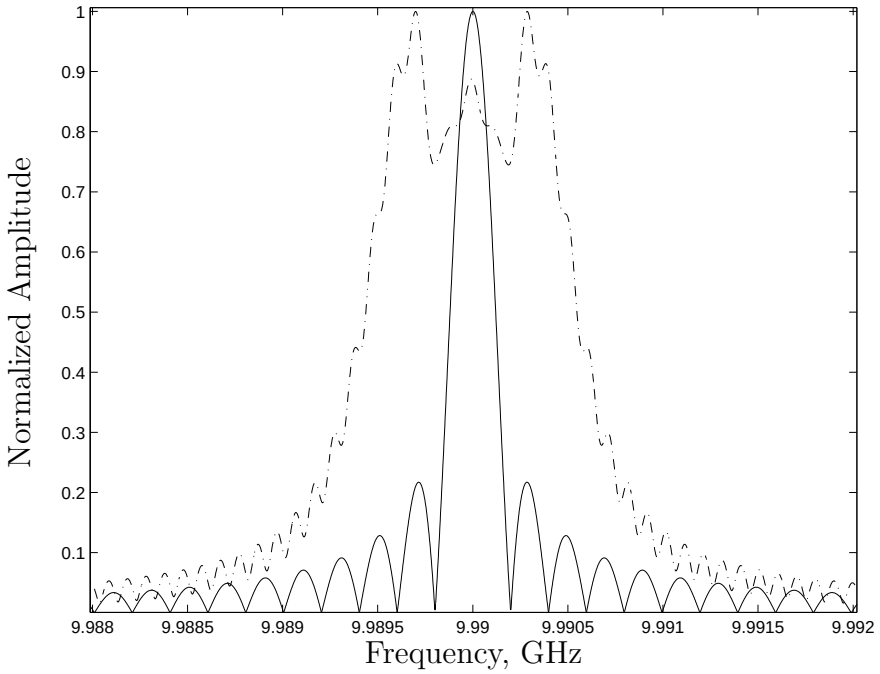

Figure 5.1: RSF waveform (solid) versus LFM-RSF waveform (dashed) frequency coverage. For a single subpulse, this LFM-RSF waveform covers substantially more frequency than last chapter's LFM-RSF waveform.

Using (5.4), the center frequency difference between subpulses Δf is

$$\begin{aligned} t_b \Delta f &= 5 && (5.9) \\ \Delta f &= \frac{5}{t_b} && (5.10) \\ \Delta f &= \frac{5}{11.11\ \mu\text{sec}} \\ \Delta f &= 450\ \text{KHz}. \end{aligned}$$

Equation (5.5) specifies the total bandwidth within each subpulse B_s as

$$\begin{aligned} t_b B_s &= 12.5 && (5.11) \\ B_s &= \frac{12.5}{t_b} \\ B_s &= \frac{12.5}{11.11\ \mu\text{sec}} \\ B_s &= 1.125\ \text{MHz}. \end{aligned}$$

Comparing the numbers from the previous two equations, there is considerable frequency overlap between successive subpulses. In [7], this paper requires the frequency overlap to remove autocorrelation function grating lobes. The final parameter to define for this waveform is the chirp rate α. The new chirp rate for each subpulse is

$$\begin{aligned} \alpha &= \frac{B_s}{2t_b} \\ \alpha &= \frac{1.125 \text{ MHz}}{2\ 11.11\ \mu\text{sec}} \\ \alpha &= 5.06 \text{ x } 10^{10}\ \frac{\text{cycles}}{\text{sec}^2}. \end{aligned} \tag{5.12}$$

When not violating the time-width product $N^2 = BT$, the chirp rate is 2.0 x 10^{10} $\frac{\text{cycles}}{\text{sec}^2}$. The increase in α makes intuitive sense considering the increase in bandwidth B_s.

All other system parameters and configurations remain unchanged from the previous chapter with the exception of the LFM-RSF subpulse duration t_b. The transmitted waveform is given by

$$s(t) = \sum_{i=0}^{N-1} e^{\left[j2\pi(f_{\text{i}}t+\alpha t^2)\right]} \qquad \text{i}\frac{T}{N} < t < (\text{i}+1)\frac{T}{N} \tag{5.13}$$

where N is the number of subpulses and f_{i} are the randomly selected subpulse frequencies between $f_c - B/2 < f_{\text{i}} < f_c + B/2$ with each subpulse having a t_b time duration.

Once more, the motive for replacing the uniform frequency with LFM chirp signals across the subpulses of the CW RSF waveform is greater frequency coverage in the $B \times T$ data region. Figure 5.2 graphically shows the LFM chirp signals on each subpulse. Greater frequency coverage correlates to filling the $B \times T$ region more completely and improving the AF approximation for sets of RSF waveforms given by

$$|\chi(T_r, f_d)|^2 = |\text{sinc}(BT_r)\text{sinc}(Tf_d)|^2, \tag{5.14}$$

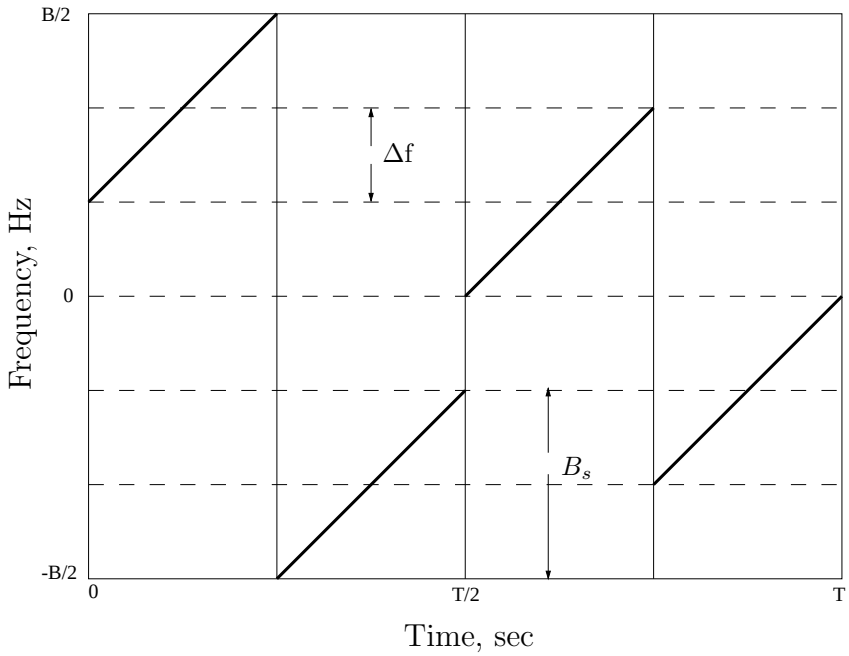

Figure 5.2: Time-Bandwidth region for LFM-RSF waveforms ($N^2 < BT$). One example of a random ordering of the subpulses. The number of subpulses N equal 4 (illustration purposes only). In the simulation, the number of subpulses equals 45. The diagonal lines in the figure represent the LFM chirp signals. This figure shows the frequency overlap between successive pulses.

where B is the system bandwidth, T_r is the time delay, T is the pulse width, and f_d is the Doppler frequency shift. It is this enhanced approximation that deepens the Doppler frequency nulls in the AF at the aliased scatterers location (integer multiples of the PRF). By increasing the null depth, this waveform increases the amount of aliased scatterer energy suppression.

From the previous chapter, the actual frequency coverage from the LFM chirp signal on the subpulses ($BT = N^2$) is not significant enough an increase compared to the frequency coverage in a fixed frequency signal. The time duration of the subpulse T/N is too short to cause a large enough frequency change across the subpulse. The consequence of a small frequency spread from an LFM chirp is a frequency coverage

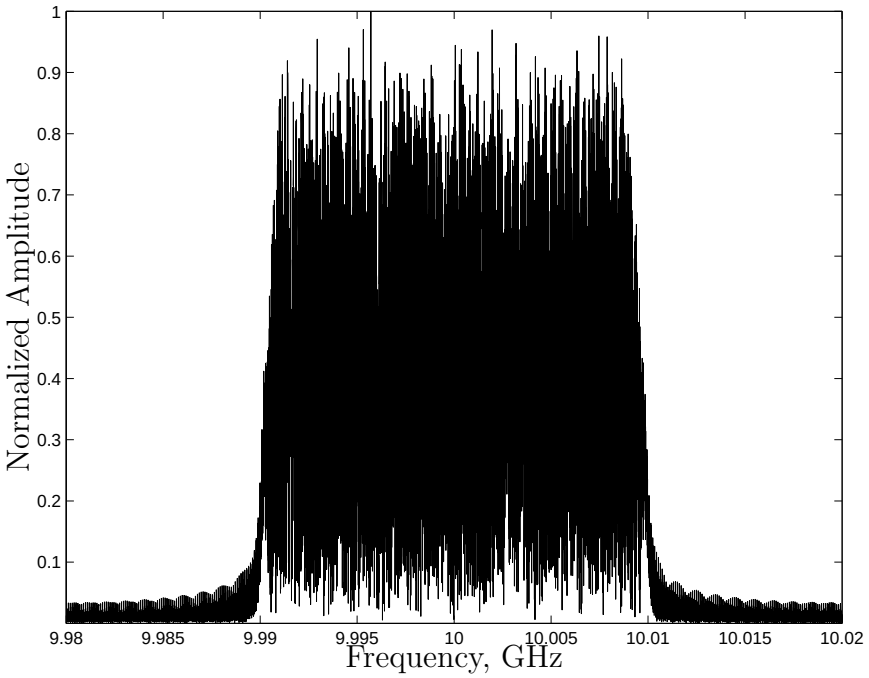

Figure 5.3: LFM-RSF Waveform Frequency Coverage for one range profile. No major gaps occur in the passband of $f_c - B/2 < f < f_c + B/2$ ensuring adequate frequency coverage.

appears more like a fixed frequency signal. The subpulse time duration, not frequency change, is the dominant cause of the spread in frequency. In this chapter, the waveform design lengthens the subpulse time duration and creates frequency overlap between successive pulses in time. These modifications allow the change in frequency to be significant enough to exhibit greater frequency coverage. Figure 5.1 verifies the frequency coverage for the LFM chirp signal across the subpulse when $N^2 < BT$ is larger than the fixed frequency signal frequency coverage.

Figure 5.3 shows the frequency coverage of one complete LFM-RSF waveform. There are no gaps in the frequency coverage. This waveform achieves the required uniform frequency coverage across the bandwidth to achieve range resolution and reject range aliasing in the range profile [11].

The AF diagram for the transmitted signal in (5.13) exhibits similar characteristics as the AF diagrams from Chapters 3 and 4. Figure 5.4(a) shows the AF after one realization of a CW LFM-RSF waveform. This figure shows the the nulls at integer

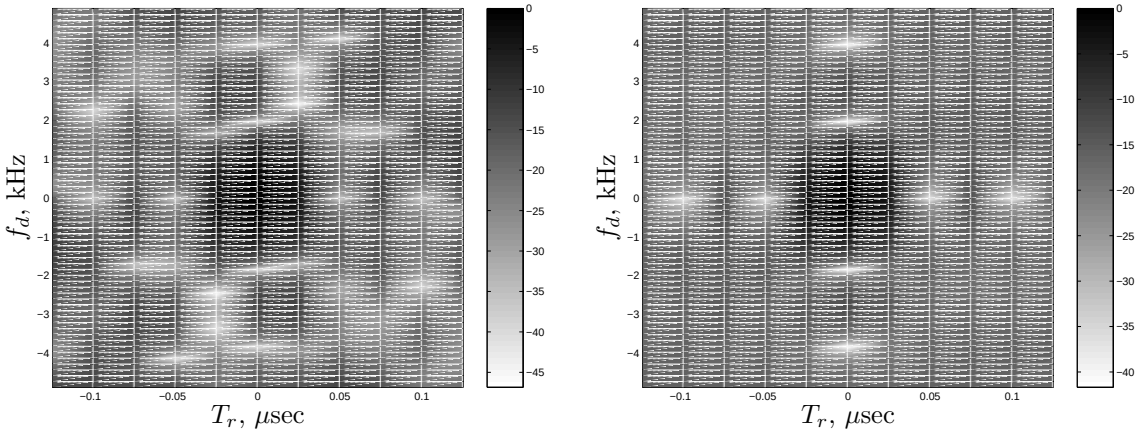

(a) (b)

Figure 5.4: (a) Ambiguity Function for One Realization of an LFM-RSF Waveform. This figure shows the noise-like Ambiguity Function for one LFM-RSF waveform [11]. Null location is correct at integer multiples of the PRF (2 KHz), but the overall 2-D sinc shape is not present.
(b) Ambiguity Function for 100 Realizations of LFM-RSF Waveforms. The set of RSF waveforms better approximate (4.2). Null location is correct at integer multiples of the PRF (2 KHz) and the ambiguity shape is similar to a 2-D sinc.

multiples of the PRF without the 2-D sinc shape as expected. Figure 5.4(b) shows the AF diagram after 100 realizations that better approximates the AF in (5.14). Again, this approximation improvement stems from filling the $B \times T$ region in Fig. 5.2 more uniformly.

5.2 Results

Through range profiles and SAR images, this section shows the effectiveness of the CW LFM-RSF waveform in removing WA-SAR Doppler aliasing.

5.2.1 Range Profile. Figure 5.5(a) shows one realization of the range profile from one synthetic aperture array location at a platform velocity of 100 m/s. A single realization of the LFM-RSF waveform fills up N of the possible N^2 squares in the $B \times T$ region given in Fig. 5.2. This single realization results in a noise-like waveform with a thumbtack AF [11]. Figure 5.5(b) shows the reference scatterer at

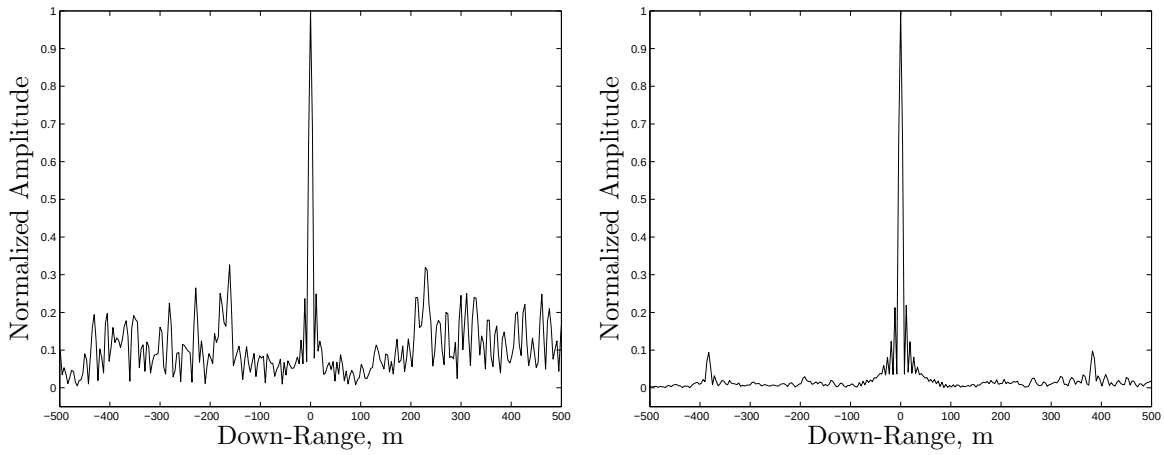

(a) (b)

Figure 5.5: (a) Range profile of one realization of LFM-RSF waveform at a platform velocity at 100 m/s. Noise from a single RSF waveform dominates much of the profile. (b) Range profile with 100 realizations. The noise floor does not dominate the range profile when compared to (a) because of the more structured nature of sets of RSF waveforms.

the correct down-range location with a relatively high noise floor due to this noise-like AF. When the number of realizations of one range profile increases to 100, the set of random realizations of the LFM-RSF waveform fills $B \times T$ region in Fig. 5.2 more uniformly and improves the approximation of the AF in (5.14). After 100 realizations of the CW LFM-RSF waveform, the reference scatterer in Fig. 5.5(b) is still at its proper location and magnitude, but the noise floor level decreases due to improved AF approximation.

Figure 5.6(a) shows the range profile after one realization of the waveform with a platform velocity of 200 m/s. Similar to $v_a = 100$ m/s, this range profile correctly resolves the reference scatterer in range with full magnitude. The noise floor is present again as expected. Figure 5.6(b) exhibits the range profile after 100 realizations of LFM-RSF waveforms. This figure illustrates the anticipated low noise floor and the absence of other scatterers due to their Doppler characteristics and (5.14).

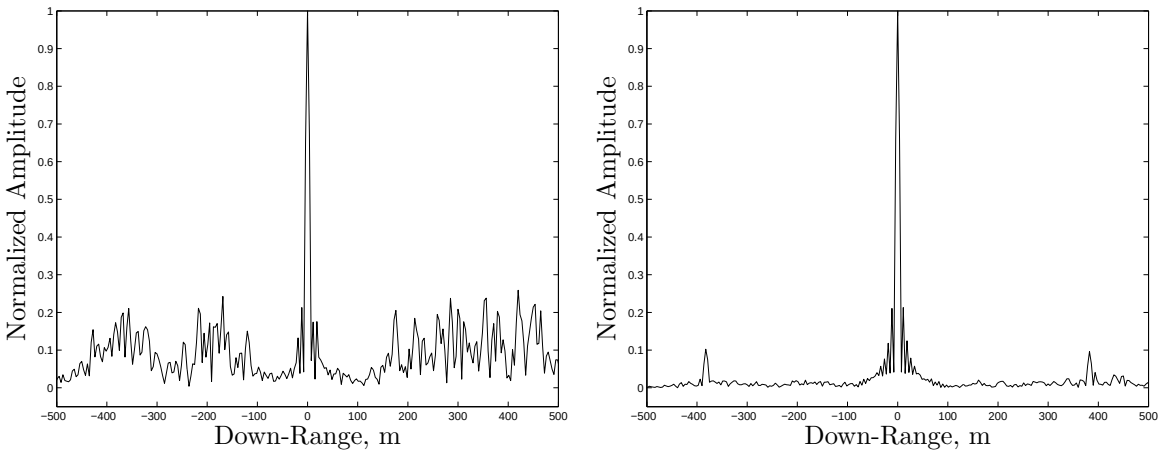

(a) (b)

Figure 5.6: (a) Range profile of one realization of LFM-RSF waveform at a platform velocity at 200 m/s. Noise from a single RSF waveform dominates much of the profile. (b) Range profile with 100 realizations. The noise floor does not dominate the range profile when compared to (a) because of the more structured nature of sets of RSF waveforms.

5.2.2 SAR Image. The application of CW LFM-RSF waveforms in the SAR research scenario result in SAR images containing only the scatterer of interest at its true location in range and cross-range with associated noise floors. The waveforms remove Doppler aliasing seen in Figs. 5.7(a) and 5.8(a). Image formation occurs via Back-Projection from processing the individual range profiles from each synthetic aperture location. Back-Projection forms the final image by summing the individual images from the range profiles. Figures 5.7(b) and 5.8(b) show the images at platform velocities of 100 and 200 ms/s respectively. Table 5.1 shows the expected scatterers that should alias into the SAR image at both platform velocities. These figures exhibit the reduction of aliased scatterers from the LFM images and a noise floor around -45 dB for $v_a = 100$ m/s and -40 dB for $v_a = 200$ m/s. Over the course of the synthetic aperture, the random nature of the set of LFM-RSF waveforms in the synthetic aperture virtually fills the $B \times T$ region in Fig. 5.2 to approximate (5.14). The waveform design effectively nulls out the scatterers at integer multiples of the PRF resulting in alias-reduced SAR images.

Table 5.1: Scatterer Normalized Doppler Parameters

	Normalized Doppler ($\overline{\omega}$) (Hz)	
Scatterer	100 m/s	200 m/s
1	2.00	4.00
2	1.50	2.99
3	0.99	1.98
4	0.50	1.00
5	0	0
6	-0.51	-1.01
7	-1.00	-1.99
8	-1.50	-3.00
9	-2.01	-4.02

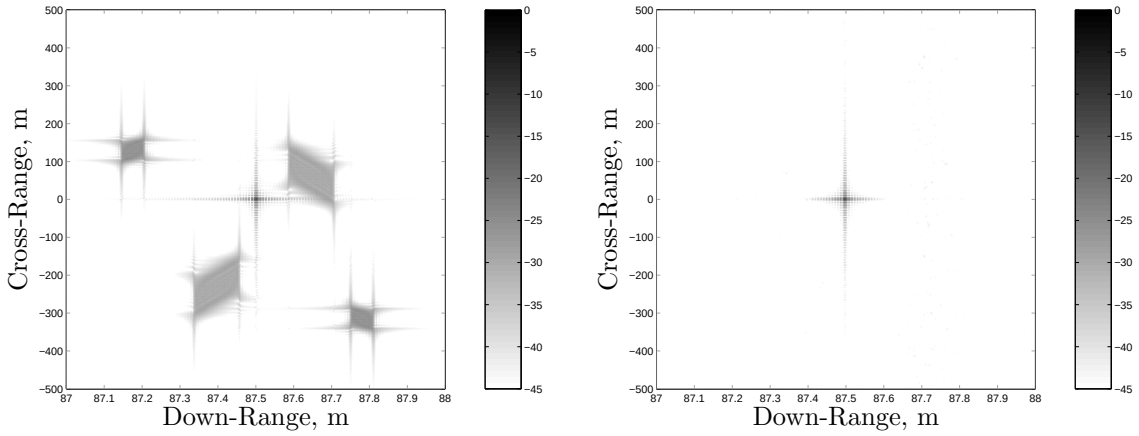

(a) (b)

Figure 5.7: (a) LFM Image at a platform velocity of 100 m/s with a -45 dB dynamic range. The scatterers that alias into the image have a Doppler frequency shift equal to an integer multiple of the PRF. 4 scatterers alias into the image in this case.
(b) LFM-RSF image at a platform velocity of 100 m/s. The LFM-RSF waveform correctly images the scatterer of interest and removes the 4 aliased scatterers.

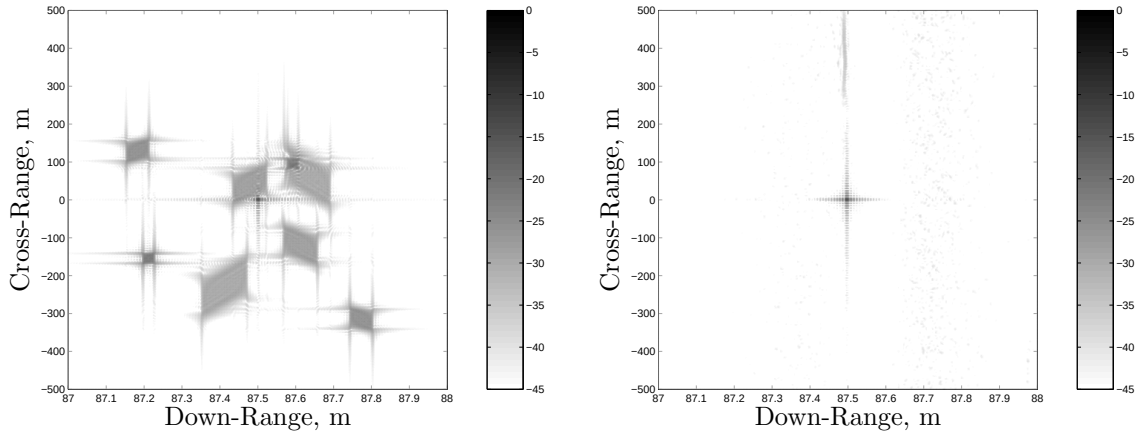

(a) (b)

Figure 5.8: (a) LFM Image at a platform velocity of 200 m/s with a −45 dB dynamic range. The scatterers that alias into the image have a Doppler frequency shift equal to an integer multiple of the PRF. All remaining scatterers alias into the image in this case.
(b) LFM-RSF image at a platform velocity of 200 m/s. The LFM-RSF waveform correctly images the scatterer of interest and removes the aliased scatterers.

In Figure 5.8(b), a noticeable mass of energy is visible on the Doppler axis ($T_r = 0$). This mass has a maximum dB magnitude of −28.83 dB corresponding to a 0.036 normalized magnitude. While it clouds a minor portion of the image, this energy mass's contribution to the overall energy value of the terrain patch is minimal at 0.036 per pixel.

5.3 Performance Metrics

Aliasing suppression by the CW LFM-RSF waveforms is obvious through visual inspection of the images. However, it is important to quantitatively understand the amount of alias reduction by this waveform.

Implementing the CW LFM-RSF waveform results in alias-reduced images. Referring to Fig. 5.7(a), the aliased scatterers are spread around the scatterer of interest in the image at $v_a = 100$ m/s. Figure 5.7(b) shows the image resulting from the implementation of the CW LFM-RSF waveform. The amount of normalized energy

Table 5.2: Normalized Energy Summary.

	Normalized Energy Reduction (%)	
Waveform	100 m/s	200 m/s
RSF	98.99	93.46
LFM-RSF ($N^2 = BT$)	99.57	91.35
LFM-RSF ($N^2 < BT$)	99.94	98.62

in this case is 1.0003. This waveform significantly reduces the amount of aliased energy from the LFM case by 99.94%. With $v_a = 200$ m/s, Fig. 5.8(a) illustrates the additional energy introduced into the terrain patch image due to the 4 extra aliased scatterers. Figure. 5.8(b) shows that a CW LFM-RSF waveform removes all aliased scatterers. This waveform reduces normalized energy to 1.011: a 98.62 % reduction in aliased energy. Table 5.2 summarizes the normalized energy reduction.

5.4 Summary

This chapter shows that implementing a CW LFM-RSF waveform in a WA-SAR system violating a time-bandwidth product produces alias-reduced images. Chapter 5 improves the frequency coverage in the $B \times T$ data region compared to chapter 4 by reducing the amount of subpulses in the RSF waveform. Referring to Fig. 5.1 and Table 5.2, the reduction in subpulses leads to a frequency coverage expected from an LFM signal and improves aliased scatterer energy reduction.

VI. Conclusions

This chapter restates the research purpose, summarizes simulation results, discusses significance of research results, and proposes additional research topics. Also, this final chapter places emphasis on research general topics and defers to previous chapters for the details.

6.1 Research Focus

The research investigates benefits of implementing a Linear Frequency Modulated Random Stepped-Frequency (LFM-RSF) waveform to reduce Doppler aliasing in a Wide-Angle SAR (WA-SAR) scenario. Previous work shows that a Random Stepped-Frequency (RSF) waveform effectively suppresses SAR image Doppler aliasing. Implementing an LFM chirp on the RSF subpulses theoretically increases subpulse frequency coverage and results in enhanced removal of aliased scatterers. This research uses computer simulation to validate the previous work and to investigate the proposed theory. Validation of the previous work verifies an accurate simulation scenario and permits comparisons to proposed theory results. Following validation, the research modifies the simulation to LFM-RSF waveforms.

6.2 Results Summary

Simulation results support both the previous work and the proposed theory through visual inspections and normalized energy metrics. Simulation results confirm aliased scatterer suppression in SAR images for RSF and LFM-RSF waveforms. Both waveforms suppress the visual effects of aliased scatterers and correctly image the scatterer of interest. Similar metric numbers for RSF and LFM-RSF waveforms indicate comparable energy suppression performance.

Since both waveforms mitigate aliased scatterers from the scene, suppressing energy from the noise floor is the primary distinguisher concerning performance between waveforms. LFM-RSF waveforms theoretically remove more energy from the noise floor. In this research, LFM-RSF waveforms suppress slightly more aliased scat-

terer energy than RSF waveforms at a platform speed of 100 m/s. At a platform speed of 200 m/s, LFM-RSF waveforms exhibit the expected aliased scatterer suppression. However, an undesired mass of energy appears on the image Doppler frequency axis. In general, the LFM-RSF waveform violating the conventional time-bandwidth constraint performs better at all platform speeds than the LFM-RSF waveform satisfying the constraint.

Similar simulation results between waveforms validates RSF theory for suppressing Doppler aliased scatterers in WA-SAR. Furthermore, simulation results indicate increasing frequency coverage by implementing LFM-RSF waveforms does improve aliased scatterer suppression. However, this improvement does depend on platform speed. The energy mass encumbers the LFM-RSF waveform images when platform speed is 200 m/s. This mass does not appear when platform speed is 100 m/s. The energy mass does appear at similar magnitudes as aliased scatterers, but evidence suggests energy clumping might result from increased aliased scatterer energy. The exact cause of the extra energy mass remains unclear.

6.3 Suggested Areas for Future Research

Additional areas of research recommend extending waveform diversity concepts or relaxing simulation assumptions. The recommendations either attempt improving the research's proposed theory or undertake other meaningful objectives in WA-SAR.

An extension to waveform diversity is amplitude weighting of returned echo signals [11]. Generating range profiles by matched filtering allows amplitude weighting since $\text{sinc}(BT_r)$ is the returned echo signal envelope where B is the system bandwidth and T_r is the range delay. Applying amplitude weighting on the echo signal reduces the range sidelobes resulting from the envelope. Depending on waveform and weighting method, the reduction in sidelobes may be significant enough to generate a less noisy image. This method widens the main lobe response; possibly reducing image resolution. Given the research objectives, resolution loss is an acceptable tradeoff for lower range sidelobes.

Another method to modify this research is changing the scenario geometry to violate the far-field assumption. Relaxing this assumption drastically changes the simplistic simulation design for electromagnetic signal propagation. If scatterers are near-field instead of far-field, returned signals must incorporate near-field electromagnetic signal effects. A near-field imaging scenario also violates the assumption the scene does not change from pulse-to-pulse. The simulation must account for noncoherent signal summation between each pulse.

This research also assumes point scatterers for targets in the scene. Point scatterers display known properties and are beneficial in proving waveform concepts. Since previous work and this research prove RSF waveforms produce alias-reduced WA-SAR images, complex geometries can replace point scatterers to investigate resolution and returned echo signal amplitude variation issues. Complex geometries include buildings, tanks, airplanes, and other structures of interest. Bandwidth and synthetic aperture length require changing to handle resolution requirements of imaging complex geometries. Complex geometries also require that fluctuating returned echo signals replace unit amplitude returned echo signals. The returned echo signal changes with the electromagnetic signal reflecting off different sections of the complex scatterer. Changing from point scatterers to complex scatterers in the simulation scene approximate real-world conditions.

Bibliography

1. Balanis, Constantine. *Advanced Engineering Electromagnetics*. John Wiley & Sons, Inc., New York, NY, first edition, 1989.

2. Carrara, Walter G., Ronald S. Goodman, and Ronald M. Majewski. *Spotlight Synthetic Aperture Radar; Signal Processing Algorithms*. Artech House, Boston, 1995.

3. Hale, Todd B. "EENG535 - Radar Systems Analysis", July 2004.

4. Harger, Robert O. *Synthetic Aperture Radar Systems; Theory and Design*. Academic Press, New York, 1970.

5. Jackowatz, Charles. *Spotlight-Mode Synthetic Aperture Radar: A Signal Processing Approach*. Kluwer Academic Publishers, Boston, 1996.

6. Levanon, N. and E. Mozeson. "Modified Costas Signal". *IEEE Transactions on Aerospace and Electronic Systems*, 39, No. 2:694–703, April 2004.

7. Levanon, Nadav and Eli Mozeson. "Orthogonal Train of Modified Costas Pulses". *IEEE, 2004 Radar Conference*, 255–259. April 2004.

8. Luminati, J. E., T. B. Hale, M. A. Temple, M. J. Havrilla, and M. E. Oxley. "Cross-Range Aliasing Artifact Reduction in SAR Imagery using Stepped-Frequency Waveforms". *Submitted to IEEE Transactions on Aerospace and Electronic Systems*, 2005.

9. Luminati, J. E. and W. Wood. "Fourier Transform and Back-Projection Methods of SAR/ISAR Imaging using Circumscribed Processing Regions". *20th Annual Review of Progress in Applied Computational Electromagnetics*, 2004.

10. Mitra, Sanjit K. *Digital Signal Processing: A Computer-Based Approach*. McGraw Hill, New York, 1998.

11. Skolnik, Merrill I. *Introduction to Radar Systems, Second Edition*. McGraw-Hill, Inc., New York, 1980.

12. Skolnik, Merrill I. *Radar Handbook*. McGraw-Hill, Inc., New York, 1990.

13. Soumekh, Mehrdad. *Synthetic Aperture Radar Signal Processing with Matlab Algorithms*. Wiley, New York, 1999.

REPORT DOCUMENTATION PAGE

Form Approved
OMB No. 074-0188

1. REPORT DATE *(DD-MM-YYYY)*	2. REPORT TYPE	3. DATES COVERED *(From – To)*
03-21-2005	Master's Thesis	Aug 2003 – Mar 2005

4. TITLE AND SUBTITLE
Doppler Aliasing Reduction In Wide-Angle Synthetic Aperture Radar Using A Linear Frequency Modulated Random Stepped-Frequency Waveform

5a. CONTRACT NUMBER

5b. GRANT NUMBER

5c. PROGRAM ELEMENT NUMBER

6. Author(s)
Jason R. McMahon, Capt, USAF

5d. PROJECT NUMBER

5e. TASK NUMBER

5f. WORK UNIT NUMBER

7. PERFORMING ORGANIZATION NAMES(S) AND ADDRESS(S)
Air Force Institute of Technology
Graduate School of Engineering and Management (AFIT/EN)
2950 Hobson Way, Bldg 641
WPAFB OH 45433-7765

8. PERFORMING ORGANIZATION REPORT NUMBER
AFIT/GE/ENG/05-11

9. SPONSORING/MONITORING AGENCY NAME(S) AND ADDRESS(ES)
Ed Zelnio
Air Force Research Lab Sensors Directorate (AFRL/SNA)
2241 Avionics Circle, Bldg 620
Wright-Patterson AFB OH 45433-7318
ph: 937-255-4949 x4211

10. SPONSOR/MONITOR'S ACRONYM(S)

11. SPONSOR/MONITOR'S REPORT NUMBER(S)

12. DISTRIBUTION/AVAILABILITY STATEMENT

13. SUPPLEMENTARY NOTES

14. Abstract
This research examines the theory, application, and results of using Random Stepped-Frequency (RSF) waveforms to mitigate Doppler aliasing in a wide-angle Synthetic Aperture Radar (SAR) imaging scenario. Severe Doppler aliasing typically occurs in this scenario since range extent requirements force the pulse repetition frequency to a value violating the lower bound for Doppler aliasing. Building on previous research, this work expands upon RSF waveform analysis using a Linear Frequency Modulated RSF (LFM-RSF) waveform. The RSF waveform suppresses Doppler aliasing by positioning nulls at the aliased scatterer location. Applying LFM with RSF processing theoretically provides greater frequency coverage and aliased scatterer cancellation improvement when compared to fixed frequency values. Results using the LFM-RSF waveform show images with alias mitigation performance consistent with previous non-LFM RSF results. Given a 45 dB image dynamic range and satisfying a time-bandwidth product criterion, the LFM-RSF waveform produces an image with aliased energy reduced by 99.6%. Slightly more energy reduction is possible by violating the time-bandwidth product criterion with an associated frequency overlap between subpulses. This violation leads to additional frequency coverage which enhances aliased energy reduction to 99.9%.

15. SUBJECT TERMS
SAR, Wide-Angle SAR, Aliasing Reduction, Pulse Compression, LFM, Waveform Diversity

16. SECURITY CLASSIFICATION OF:			17. LIMITATION OF ABSTRACT	18. NUMBER OF PAGES	19a. NAME OF RESPONSIBLE PERSON
REPORT	ABSTRACT	c. THIS PAGE			Maj Todd B. Hale (todd.hale@afit.edu)
U	U	U	UU	100	19b. TELEPHONE NUMBER *(Include area code)* 937-255-3636 x4639